Improving Galactic Center Astrometry by Reducing the Effects of Geometric Distortion

S. Yelda[1], J. R. Lu[2], A. M. Ghez[1,3], W. Clarkson[1], J. Anderson[4]

ABSTRACT

The recent advent of adaptive optics systems on 8-10 m class telescopes has allowed for sub-milliarcsecond astrometry from the ground on a wide variety of astronomical objects. However, while the relative astrometry of the Galactic center is currently limited to a mere $\sim$0.2 mas, the *absolute* astrometry in this region has been limited to $\sim$6 mas at Keck. In this paper, we identify and correct major limitations to our absolute astrometry - geometric optical distortion and differential atmospheric refraction. These effects introduce $\sim$1-5 mas scale distortions over the spatial scales of the SiO masers that are used to define the absolute reference frame for proper motions of stars at the GC. With new observations of M92 at a wide variety of positions and orientations, we improve upon existing geometric distortion solutions for the NIRC2 narrow camera at the W. M. Keck II 10 m telescope. Post-fit residuals are reduced by a factor of $\sim$2-4 over previous solutions. Our relative astrometry can now be tied into an absolute radio reference frame to within $\pm$0.07 mas/yr, allowing us to better test the possibility of a relative motion between the central black hole and the stellar cluster. We have constrained this motion to less than 13 km/s and 21 km/s in the East-West and North-South directions, respectively. The gains in our astrometric accuracy will also improve our ability to measure relatively small stellar accelerations at large radii. This distortion solution is available to the public in the form of FITS files.

1. Introduction

High angular resolution astrometry has been a very powerful technique for studies of the Galactic center. Over the last decade, it has revealed a supermassive black hole (Eckart & Genzel

[1]UCLA Department of Physics and Astronomy, Los Angeles, CA 90095 -1547; syelda, ghez@astro.ucla.edu

[2]Astrophysics, California Institute of Technology, MC 249-17, Pasadena, CA 91125; jlu@astro.caltech.edu

[3]UCLA Institute of Geophysics and Planetary Physics, Los Angeles, CA 90095-1565

[4]Space Telescope Science Institute, 3700 San Martin Drive, Baltimore, MD 21218; jayander@stsci.edu

1997; Ghez et al. 1998), a disk of young stars surrounding the central supermassive black hole (Levin & Beloborodov 2003; Genzel et al. 2003; Paumard et al. 2006; Lu et al. 2009), and an eccentric orbit for the Arches, a massive young star cluster located at a projected galacto-centric distance of 30 pc (Stolte et al. 2008). While the speckle imaging work carried out on the Galactic center in the 1990's had typical centroiding uncertainties of $\sim$1 mas, recent deep, adaptive optics (AO) images have improved the precision of stellar centroiding by a factor of $\sim$6-7, significantly increasing the scientific potential of astrometry at the Galactic center (Ghez et al. 2008; Gillessen et al. 2009). Further gains in astrometric precision could lead to ultra-precise measurements of the distance to the Galactic center (R_o), measurements of individual stellar orbits at larger galacto-centric radii, and, more ambitiously, to measure post-Newtonian effects in the orbits of short-period stars (e.g., Jaroszyński 1998, 1999; Salim & Gould 1999; Fragile & Mathews 2000; Rubilar & Eckart 2001; Weinberg et al. 2005; Zucker & Alexander 2007; Kraniotis 2007; Nucita et al. 2007; Will 2008).

Two factors that currently limit astrometric measurements of stars at the Galactic center are (1) the level to which AO cameras' geometric distortions are known and (2) differential atmospheric refraction (DAR), which has not yet been explicitly corrected for in any Galactic center proper motion study (Ghez et al. 2008; Gillessen et al. 2009). While optical distortion from an infrared camera is expected to be static, distortion from the AO system and the atmosphere not corrected by AO, is not. Initial estimates of the optical distortions for AO cameras are generally based on either the optical design or laboratory test, which do not perfectly match the actual optical distortion of the system. Both uncorrected camera distortions and DAR leave $\sim$1-5 mas scale distortions over the spatial scales of the SiO masers that are used to define the absolute reference frame for proper motions of stars at the Galactic center (see e.g., Reid et al. 2007). These are significantly larger than the $\sim$0.2-0.3 mas precision achieved in the relative astrometry of Ghez et al. (2008) and Gillessen et al. (2009). While the impact of all these effects on relative astrometry has been minimized by mapping the coordinate systems of different epochs of observations to a reference set of measurements, allowing $\sim$0.2-0.3 mas precision in the relative astrometry to be achieved, the full impact of these effects is imposed on absolute astrometric measurements. Therefore, correcting these effects would have the greatest improvement on absolute astrometric measurements. However, relative astrometry would also be improved by eliminating these effects before the images, which are obtained at different times and occasionally different orientations, are combined.

In this paper, we identify and correct for two effects that currently limit the astrometric accuracy and precision of Keck AO measurements of the Galactic center. Specifically, we (1) obtain a new, publically-available distortion solution for the infrared imaging camera behind the Keck AO system (NIRC2) and (2) correct for DAR. Furthermore, having corrected for these effects, we present a set of absolute astrometric measurements of infrared stars within 0.″5-10" of the central

black hole that can be used to define the absolute reference frame of narrow field Galactic center (GC) measurements that do not contain enough of the SiO radio masers. We place limits on the relative motion between Sgr A* and the nuclear stellar cluster. Section 2 presents observations and analysis of the globular cluster, M92, that were used to derive the first distortion solution for NIRC2 that is based on on-sky measurements, as opposed to NIRC2's internal pinhole mask. In section 3 we apply this solution, along with corrections for DAR, to observations of the GC and show that our absolute astrometry is improved to $\sim$1 mas. With such improved accuracy, we have a greater ability to test the motion of the central black hole with respect to the stellar cluster and constrain the relative motion to <17 km/s ($\sim$0.5 mas/yr). While this work has been carried out in the context of the Galactic center, the new distortion solution also benefits a wide array of other science that is currently being carried out with NIRC2, including astrometric studies of extrasolar planets (Marois et al. 2008), brown dwarf binaries (Konopacky et al. 2007; Liu et al. 2008; Dupuy et al. 2008) and compact objects (Cameron & Kulkarni 2007).

2. Observations & Analysis

2.1. M92 (Keck)

Observations of the globular cluster M92 (NGC 6341; α = 17 17 07.27, δ = +43 08 11.5) were made from 2007 June to 2009 May using the AO system on the W. M. Keck II 10 m telescope with the facility near-infrared camera NIRC2 (PI: K. Matthews). All images were taken with the narrow field camera, which maps the 1024$\times$1024 pix array into $\sim$10"$\times$10" field of view, and through the K' (λ_0=2.12 μm, $\Delta\lambda$=0.35 μm) band-pass filter. While the Natural Guide Star adaptive optics (NGS-AO) system was used to obtain the majority of the data, the Laser Guide Star (LGS) AO system was used for one run in 2008 June. The NGS-AO atmospheric corrections and the LGS-AO low-order, tip-tilt corrections were made using visible observations of USNO-B1.0 1331-0325486 (R = 8.5 mag). The atmospheric conditions and AO corrections for the observations yielded point spread functions (PSFs) that, on average, had Strehl ratios of $\sim$0.55 and FWHM of $\sim$50 mas.

M92 was observed at 79 different combinations of position angles (PAs) and offsets (see Figure 1), with three identical exposures taken at each pointing. This allowed for a given star to fall on several different parts of the detector over the course of the observations. We note that the PA (θ) convention used here is such that the stars are rotated clockwise by an amount θ (i.e., the camera is rotated counter- clockwise). The field of view of NIRC2's narrow camera contained the Natural Guide Star (NGS) in each pointing, and in most cases two other nearby stars, which are circled in Figure 2; this facilitated the process of combining the positional information from all of the different pointings. Empirical centroiding uncertainties are estimated using the three images

at each pointing and computing the RMS error of each star's position. The typical centroiding uncertainty is $\sim$0.02 pix ($\sim$0.2 mas). Table 1 provides the details of the NIRC2 M92 observations.

The M92 images are calibrated and stellar positions are measured from these images using standard techniques. Specifically, the images are first dark- and sky-subtracted, flat-fielded, and bad-pixel and cosmic ray corrected. The images are then run through the point spread function (PSF) fitting program *StarFinder* (Diolaiti et al. 2000), which is optimized for adaptive optics observations of crowded stellar fields to identify and characterize stars in the field of view. *StarFinder* iteratively constructs a PSF from a set of bright stars in the field, which have been pre-selected by the user. For M92, a total of 16 stars spread out across the detector are used to obtain a PSF that is representative of the entire field. The resulting PSF is then cross-correlated with the image and detections with a correlation peak of at least 0.7 are considered candidate stars. Relative astrometry and photometry are extracted by fitting the PSF to each candidate star. This results in a star list for each of the 237 NIRC2 images.

Final star lists for each pointing are produced by combining each set of three star lists from images with the same observational setup. Three initial criteria are used to trim out fake or problematic source detections. First, only stars detected in all three images are kept, with final positions that correspond to that from the first image. Second, we remove the two brightest stars (the NGS and a comparably bright star $\sim$5.1" to the east that appears in the images of 147 out of 237 pointings) and any other source identified within a 60-pixel radius of these stars (see Figure 2). The bright sources are $\sim$1 mag brighter than any other detected star and are often detected at levels that saturate the detector. Saturation leads to poor PSF matching with the empirical PSF estimate, and consequently poor positional estimates for these two stars, as well as $\sim$20-50 false detections in their halos. With these selection criteria, the 79 final star lists contain a combined total of 3846 stellar positions.

2.2. M92 (HST ACS/WFC)

To characterize the optical distortion in the NIRC2 camera, it is ideal to compare the measured set of stellar positions to those in a distortion-free reference frame. As this reference frame does not exist, we choose observations of M92 made with the Advanced Camera for Surveys (ACS) Wide Field Channel (WFC), which has a plate scale $\sim$49.993 $\pm$ 0.001 mas/pix and position angle offset = -0.0038° $\pm$ 0.0011° (van der Marel et al. 2007), as our reference frame. The distortions in this camera have been removed down to the $\sim$0.01 pix ($\sim$0.5 mas) level (Anderson 2005; Anderson & King 2006; Anderson 2007) and is therefore a useful reference for our purposes given the level of distortion in the NIRC2 camera.

HST observations of M92 were made on 2006 April 11 with both the F814W (*I*) and F606W (*V*) filters as part of the ACS Survey of Globular Clusters (GO-10775, PI: A. Sarajedini). The details of the observations, data reduction, and the construction of the M92 astrometric reference frame can be found in Anderson et al. (2008), while the catalog of positions themselves will be made available in future papers and the World Wide Web.

3. Results

3.1. A New Distortion Solution for NIRC2

To find the best fit model for NIRC2's geometric optical distortion from the M92 observations, one must account for the fact that the ACS/WFC data do not suffer from differential atmospheric refraction (DAR; see A), while the NIRC2 data come from ground-based observations and therefore will be affected by the earth's atmosphere (see Figure 4). Differential atmospheric refraction will compress an image, causing the apparent separation between a pair of stars to be smaller than their true separation. Since the stellar positions are first geometrically distorted by the atmosphere and then the telescope/instrument, it is best to "undo" these effects in the reverse direction. During the data reduction process, it is therefore optimal to first correct for optical distortion, then remove DAR from the images before comparing with HST data. In contrast, the optical distortion should be solved for using data that still have the effects of DAR included in the images. We therefore choose to add DAR to the ACS/WFC star list. Because the effects of DAR depend on the elevation and, to a much lesser extent, the atmospheric conditions of the observations, it is necessary to create a separate DAR-transformed ACS/WFC star list for each NIRC2 star list. To account for DAR, we follow the prescription for DAR given in Gubler & Tytler (1998)). Again, the stellar positions are only corrected for achromatic DAR, as the error from chromatic DAR is negligible relative to the residual distortion in ACS/WFC ($\sim$0.5 mas). Overall, the magnitude of this effect over the range of elevations for the M92 observations is expected to be $\sim$2-4 mas across NIRC2's 10" field of view, along the elevation axis.

Each of the NIRC2 star lists is then used as a reference coordinate system into which the ACS/WFC star list is transformed. In the alignment process, the ACS/WFC star list is transformed by minimizing the error-weighted (NIRC2 positional errors), net displacement for all the stars, allowing for translation, rotation, and a global plate scale. This process is described in greater detail in Ghez et al. (2008) and Lu et al. (2009). Only sources that are cross-identified in both the NIRC2 and ACS star lists are used in the remaining analysis. From the 79 separate alignments, a total of 2743 matches in stellar positions are obtained.

The mapping of ACS positions to NIRC2 positions shows clear spatial structure across the

detector, as expected from optical distortion (see Figure 5). However, some vector deviations are inconsistent with those in their immediate surroundings. These deviant measurements are found by examining the vector deviations in 205×205 pixel bins and determining the average and standard deviation. Any 3σ outliers in either the X or Y direction are removed. A total of 75 measurements are removed based on this criterion. An additional cut (>3σ) in each of these bins is made on NIRC2 positional uncertainties, as they may vary with respect to detector position. This cut removes 73 data points, four of which were also eliminated by the first cut. These bins are examined a second time for vector outliers, as they often show a rather wide distribution. The average and standard deviation in each bin are recalculated and the vector outliers (>3σ) are removed once again. This resulted in an additional loss of 26 measurements.

Many of the eliminated measurements come from common stars or images. We therefore remove all measurements of the 9 out of 150 stars and of the 8 out of 79 images that were eliminated more than 20% of the time by the sigma-clipping process. Many of these problematic stars have close neighbors (< 0.″2) that are not resolved or not well measured in the lower-resolution ACS observations ($\theta \sim$70 mas for the F814W observations). Similarly, the majority of the rejected frames, have exposure times less than 10 sec, while the remaining frames are at least 30 sec. This results in significantly higher centroiding uncertainties, residual atmospheric effects, and fewer stars detected. Although the 2008 April data set had relatively long exposure times (t_{int} = 48 sec), the observations were heavily impacted by clouds and the AO system was often unable to remain locked on the NGS. Our final data set consists of 2398 positional deviations between ACS and NIRC2, with typical centroiding uncertainty for the NIRC2 images of 0.02 pix (∼0.2 mas). The vector plot for this cleaned sample is shown in the bottom of Figure 5.

A bivariate B-spline is fit to the distortion map (Figure 5) using the SciPy package interpolate, and a look-up table sampled at each of the 1024×1024 NIRC2 pixels is subsequently produced. The effect of the smoothing factor (f; which is related to the number of nearest-neighbor measurements used to calculate the smoothing) used in the interpolating routine was investigated extensively in order to find a good compromise between the closeness of fit and the smoothness of fit. The residuals between the original distortion vectors in the bottom panel of Figure 5 and the computed shift at the nearest pixel (from the smoothed look-up table) were measured. The median deviation is found to increase until $f \sim$150, where it plateaus at a value of ∼0.27 pix. We choose for our interpolation the smoothing factor that gave nearly the lowest median deviation, f = 135. Although the deviations were lower for distortion solutions created with smaller smoothing factors, the edge effects were prominent in the look-up tables and the distribution of deviations was much larger (see Dierckx (1995) for details on surface fitting and the choice of smoothing factors). The resulting look-up tables for shifts in X and Y are shown in Figure 6, and are produced in the form of FITS files that may be fed into the IRAF routine, *Drizzle* (Fruchter & Hook 2002), to correct for the optical distortion.

Uncertainties in the distortion solution were computed by running 1000 Monte Carlo simulations, in which the data were sampled with replacement. The RMS error with respect to the distortion solution (i.e., the actual distortion solution was taken as the average) was calculated at each pixel and the results are shown in Figure 7. The average errors in X and Y are 0.05 pix and 0.04 pix ($\sim$0.4, $\sim$0.5 mas), respectively. We can see the uncertainties are highest near the edge of the detector, where less data exist. The uncertainties are also shown in the form of a histogram in Figure 8 along with a histogram of the distortion solution itself.

To solve for the global plate scale and orientation that results from this new solution, we re-reduce the raw NIRC2 observations of M92 from 2007 July, and apply corrections for distortion and DAR to these images. The distortion correction and DAR correction are applied to each image at the same time in the form of look-up tables using the *Drizzle* algorithm as implemented in IRAF (Fruchter & Hook 2002). The look-up tables are specified in *Drizzle* using the *xgeoim* and *ygeoim* keywords and are FITS files of the same dimensions as the science image. These look-up tables are created by first including the distortion solution and then applying the necessary DAR correction. Two FITS files, one for shifts in X and one for shifts in Y, are created for each NIRC2 observation and contain the shifts to be applied to each pixel in the image. From these distortion- and DAR-corrected NIRC2 images, star lists were generated and aligned to the original ACS starlist (without DAR) as described above. The resulting plate scale is $\langle s \rangle = 9.948 \pm 0.001_{stat} \pm 0.001_{abs}$ $\mathrm{pix}_{NIRC2}/\mathrm{pix}_{ACS/WFC}$. The difference between the orientation given in the header of the NIRC2 images (90° for this data set) and the measured orientation is on average $\sim 0.256^\circ \pm 0.006^\circ_{stat} \pm 0.001^\circ_{abs}$, where the absolute errors are the uncertainties in the ACS/WFC plate scale and orientation angle (van der Marel et al. 2007). Thus, the NIRC2 columns must be rotated eastward of North by 0.256° to be aligned with ACS[1].

3.2. Application to the Galactic Center

We apply the new distortion solution and DAR corrections to our existing Keck/NIRC2 Galactic center observations to both determine the accuracy of our new solution (§3.2.1) and to obtain a new and substantially improved IR absolute reference frame (§3.2.2). In the analysis described below, distortion and DAR are corrected in the data reduction process, which utilizes *Drizzle*, as explained in §3.1.

---

[1]The NIRC2 FITS header keyword for the position angle, ROTPOSN, includes a +0.7° offset, the observatory value for the angle offset of NIRC2. We have subtracted this 0.7° in our analyses. Thus, the 0.256° rotation is *in addition* to the 0.7° rotation.

3.2.1. Testing the New Model for NIRC2 Distortion

The accuracy of our distortion solution is examined using two separate LGS-AO GC data sets, both of which are described in Ghez et al. (2008), and compared with two previous estimates, which we refer to as "pre-ship" and "PBC". The pre-ship solution[2], which is good to ∼4 mas, was found using a pinhole mask, and is in the form of a 3rd-order polynomial. The more recent solution by P. B. Cameron, also from a pinhole mask, is a 4th-order polynomial and improves upon the former solution mainly along the X axis[3].

First, we use the two high precision data sets taken of the central 10"×10" on 2007 May 17 and May 20 at two different PAs (0° and 200°) with roughly the same central position. The NIRC2 positional uncertainties (δ_{pos}) for the PA=0 and PA=200 images are ∼0.022 pix and ∼0.036 pix, respectively. The PA=200 image was transformed into the PA=0 image's coordinate system, again allowing for translation, rotation, and global plate scale. The differences in the aligned positions of stars with K<14.5 are shown in Figure 9. Our new solution shows significantly less residual structure than the previous solutions. To estimate the magnitude of the residual distortion, we remove the positional measurement bias and account for the contribution from the two images used. This results in estimates of the residual distortion, of σ_r = 0.156 pix, 0.321 pix, and 0.344 pix for the new, PBC, and pre-ship solutions, respectively, While this analysis shows the improvement and the residual distortion, it mixes the residual distortions in the X and Y dimensions due to the rotation of the images.

To characterize the residuals in X and Y separately, we use widely-dithered GC data taken in 2006 May and 2008 May at PA=0, which maintains the independence of the X and Y axes. These data are described in Ghez et al. (2008) as part of their absolute astrometry analysis and have an average centroiding uncertainty (δ_{pos}) of 0.067 pix. Only four overlapping fields, each of which was imaged three times and whose centers are the corners of a 6"×6" box, were examined from this data set. The full mosaic is shown in Figure 10. *StarFinder* was run at a correlation of 0.9 on each image to create a star list, and only stars detected in at least 6 of the 12 images (and therefore at least two of the four overlapping fields) were kept in the analysis. Offsets between IRS16SW-E (which was in each of the four fields) and each of the detected stars was computed. The standard deviation of each star's offset from IRS16SW-E was taken as the positional error. The RMS offsets (σ_x, σ_y) for these solutions, shown in Figure 11, are (0.13, 0.17) pix, (0.14, 0.32) pix, and (0.41, 0.34) pix, for the new, PBC, and pre-ship solutions, respectively. These values are corrected for positional measurement bias. The new solution was found to significantly improve

[2]http://www2.keck.hawaii.edu/inst/nirc2/preship_testing.pdf

[3]http://www.astro.caltech.edu/∼pbc/AO/distortion.pdf

positional errors overall as compared to both of the previous solutions and in particular, it is a factor of 2 better in the Y direction over the most recent PBC solution.

*3.2.2. Absolute Astrometry of the GC and the Apparent Motion of Sgr A**

Measuring the relative motion between the Galaxy's central black hole and the stellar cluster in its vicinity with high precision can help refine current estimates of the distance to the Galactic center and mass of the black hole. In Ghez et al. (2008), the motion of Sgr A* was derived from the orbit of the star S0-2 in the *relative* reference frame. The best-fit orbit allowed for a proper motion of Sgr A* of $V_x = 17 \pm 11$ km/s and $V_y = 16 \pm 6$ km/s relative to the stellar cluster. This motion may arise from the gravitational influence of a massive companion, or from a systematic effect produced by improper alignment of the central 10" images. To determine if there is a true relative motion between Sgr A* and the stellar cluster, the relative positions must be transformed into an *absolute* reference frame.

Our new distortion solution allows us to improve the absolute astrometric coordinate system for narrow field (r_{sgra} < 10") imaging at the GC through IR observations of seven SiO masers detected at IR and radio wavelengths at $r_{sgra} \sim$ 5"-15" (Reid et al. 2003, 2007). We use all the data presented in Appendix C of Ghez et al. (2008) as well as two additional data sets, which were obtained in 2008 May and 2009 June with the same setups as the earlier data sets with the exception that the 2009 observations were ∼0.5 magnitude deeper in the K'-band. We re-reduced these five data sets with the new distortion solution. Mosaics from each of the 9 dithered data sets were constructed in the same way described in Ghez et al. (2008), resulting in 22"×22" images (see Figure 10). *StarFinder* was run on each IR mosaic to create a star list for each epoch with positions in NIRC2 pixel coordinates. Along with this, we also constructed a corresponding distortion uncertainty mosaicked map based on the Monte Carlo simulations (§3.1; Figure 7) and calculate the distortion error contribution to each pixel in the maser mosaic. In the overlapping areas, we compute the distortion error contribution as

$$\sigma_{dist} = \sqrt{\frac{\sigma_1^2 + \sigma_2^2 + \ldots + \sigma_N^2}{N}} \quad (1)$$

where N is the number of overlapping fields, which can vary between 1 and 4. The IR uncertainties in each mosaic's star list include the centroiding error, distortion error, and the residual distortion (0.15 pix), summed in quadrature. Radio maser positions were propagated forward using velocities from Reid et al. (2007) to create a star list at the epoch of each IR mosaic. Each of the five infrared mosaics were aligned to the radio maser star list by minimizing the error-weighted, net displacements for the masers. Errors in the transformation to absolute coordinates were determined using a jackknife sampling technique, in which one maser at a time is excluded from the alignment.

After aligning the infrared star lists to the radio, new star lists are produced in the *absolute reference frame* with Sgr A*-radio at rest at the origin. The resulting IR positions and radio maser positions are, on average, within XX σ of each other (Table 2). Line fits to these results provide estimates of the absolute positions and proper motions of the masers as well as other stars detected in the infrared mosaics. As Sgr A*-IR is not reliably detected in these shallow mosaics, we take the average alignment error of the stars in the central arcsec, 0.54 and 0.83 mas in X and Y, respectively, as the uncertainty in the position of Sgr A*-radio in the infrared maser mosaic. The plate scale and angle offset of NIRC2 determined by the transformation between the infrared and radio reference frame is shown in Table 3. The average NIRC2 plate scale and angle offset are 9.953 ± 0.001 mas/pix and $0.256 \pm 0.003^{\circ}$, respectively. This is statistically consistent with the values obtained from the ACS/WFC to NIRC2 transformation from the 2007 July data set (§3.1). The absolute proper motions were computed by fitting a linear model to the positions over time for all the stars in the five maser star lists.

The positions and velocities of a set of *infrared absolute astrometric standards* are reported in Table 4. These standards were defined as stars that (1) are detected in all 5 maser mosaics, (2) are outside the central arcsecond (r > 0.5") to reduce the effects of non-linear motions over time, (3) are brighter than K=15, (4) have velocities below 15 mas/yr and velocity errors below 5 mas/yr, (5) have reasonable velocity fits (χ^2/dof) < 4 (Ghez et al. 2008), and (6) have been spectroscopically identified as late-type stars by Do et al. (2009) and Genzel et al. (2000). This last criterion is used in order to eliminate the known net-rotation of the young stars (Genzel et al. 2000). The average positional uncertainty for these astrometric standard stars is 0.9 mas.

For the relative proper motions, we used nine data sets of the central 10" of the Galaxy obtained from the W. M. Keck Observatory between 2006 May and 2009 July. Five of these are described in Ghez et al. (2008) and the four more recent observations were taken with identical setups as these earlier observations. The data reduction and analysis procedure are also described in Ghez et al. (2008) but we note that we used the new distortion solution and corrected for DAR in this analysis. The relative reference frame is established by aligning the IR images to each other using a set of "coordinate reference" stars. This procedure effectively puts the stellar cluster at rest. Star lists from each epoch were transformed into the 2007 August data set's coordinate system, and linear models were fit to the stars' positions as a function of time.

The stars' proper motions as measured in the radio reference frame (*absolute*) can be compared to their proper motions measured in the infrared frame (*relative*) in order to determine whether there is relative motion between the two. Since Sgr A* is defined to be at rest in the radio reference frame, a velocity difference between the absolute and relative reference frames may imply that either Sgr A* is moving with respect to the cluster, or the cluster itself has a non-zero net motion.

Figure 12 shows the difference between absolute and relative velocities for 211 stars matched across the two reference frames. The outliers in the velocity differences are due to stars at relatively large distances (r $\gtrsim$ 5") from Sgr A*. The average of the velocity differences is (for X and Y, respectively) 0.14 $\pm$ 0.07 and 0.38 $\pm$ 0.06 mas/yr, where the uncertainties are the standard deviation of the mean. Thus, we detect a significant motion between the cluster and the black hole in the North-South direction. This constraint on the relative motion is an order of magnitude improvement over our previous work (see Appendix C in Ghez et al. (2008)). The motion of the black hole relative to the cluster derived from the best-fit orbit of the central arcsecond star, S0-2, in Ghez et al. (2008) was V_x = 0.4 $\pm$ 0.25 mas/yr and V_y = 0.39 $\pm$ 0.14 mas/yr (where positive velocities are towards the East and the North for X and Y, respectively). This velocity is shown as the bar in Figure 12. The velocities determined by these two methods are consistent within the uncertainties.

4. Additional Sources of Uncertainty

The residual distortion of $\sim$0.15 pix must come from sources of uncertainty that are not accounted for in our analysis. These may include uncertainties in the ACS/WFC positions, residual distortion in the ACS/WFC camera, PSF variations in the NIRC2 images, chromatic DAR, time-variable distortion, or a difference between NGS and LGS AO data.

To test the stability of the camera's distortion, we created a distortion solution with data points from 2007, the year with the most data (N=1711). A smoothing factor of f = 120 was used for the spline fitting and was determined in the same manner as our new distortion solution. Differences between data in the individual years and the 2007-only distortion solution show no significant differences, suggesting that the distortion solution is relatively stable.

While the new distortion solution represents a significant step forward in our astrometric capabilities, it still leaves $\sim$0.15 pix or $\sim$1.5 mas residual distortion in the LGS-AO GC images. Our distortion solution was computed using only NGS data, as the six LGS frames from 2008 June were thrown out based on the cuts mentioned in §3.1. To test the possibility that the NGS and LGS AO system have different distortion solutions, we compare Galactic center data taken in both LGS and NGS modes, but otherwise the same setup and in the same night in 2008 May. The data were reduced using the usual data reduction steps (see Ghez et al. (2008)), and final LGS- and NGS-only images of the Galactic center were produced. The astrometric precision for each of these images was 0.018 pix (NGS) and 0.021 pix (LGS) for stars with K < 15. The LGS image was transformed into the NGS image's coordinate system allowing only for translation between the two frames. The RMS difference in the aligned positions was $\sim$0.06 pix (1σ), which is comparable to the error in the distortion solution ($\sim$0.05 pix, Figure 8). Thus, given the uncertainties in the distortion

solution, we do not see a difference in the astrometry from images taken in NGS or LGS mode and conclude that this adds only a small contribution to the residual distortion.

The residual distortion in the ACS/WFC is measured to be ∼0.05 pix. Furthermore, while we account for achromatic DAR (typically ∼0.3 pix), *chromatic* DAR usually has ∼20 times less of an effect (∼0.02 pix; see Gubler & Tytler (1998)). If we add the above sources of error in quadrature, including the 0.06 pix error from the NGS to LGS comparison, we find a total contribution of 0.08 pix. Thus, approximately half of the residual distortion may come from these various systematics. We also note that PSF variations over the field of view may contribute additional error to our astrometry, as we have assumed a constant PSF over the field of view.

5. Conclusions

We have improved upon existing geometric distortion solutions for the NIRC2 camera at the W. M. Keck II telescope. In all tests that were performed, the new distortion solution shows an improvement by a factor of ∼2-4 over existing solutions. We take as our final residuals: (Δx_{rms}, Δy_{rms}) ∼ (0.13, 0.17) pix.

The transformations between the ACS/WFC and NIRC2 reference frames yield a relative NIRC2 plate scale of $\langle s \rangle$ = 9.948 ± 0.001_{stat} ± 0.001_{abs} $\mathrm{pix}_{NIRC2}/\mathrm{pix}_{ACS/WFC}$ and a position angle offset of $\sim 0.256^\circ \pm 0.006^\circ_{stat} \pm 0.001^\circ_{abs}$. The plate scale and angle offset obtained using Galactic center infrared data tied to the radio reference frame are statistically consistent with these values (9.953 ± 0.001 mas/pix and 0.256 ± 0.003°).

The Galactic center absolute reference frame is now known at the < 1 mas level. We present a set of *absolute astrometric standards* within 0.″5-10" of Sgr A* that can be used to define the absolute reference frame of narrow field Galactic center (GC) measurements that do not contain enough of the SiO radio masers. In comparing the stars' absolute velocities as measured in the radio reference frame to their relative velocities, we have constrained the motion between the supermassive black hole, Sgr A*, and the nuclear stellar cluster to <13 km/s in the East-West direction and <21 km/s in the North-South directions (3σ).

Improvements to the NIRC2 distortion solution may be made by increasing the number of positional measurements used to derive the solution in order to more fully sample the detector. Another source of error in our solution is the residual distortion in ACS/WFC (∼0.5 mas), and thus a self-calibrated distortion solution (Anderson & King 2003) may improve the solution further. The use of a single point spread function across the field is also a rather significant source of error, as the quality of the AO correction is best at the location of the laser and gets worse further away, leading to a spatially-variable PSF. Assuming a uniform PSF will therefore cause errors in

positional measurements. To minimize this effect, we are currently developing an algorithm to create a location-dependent point spread function.

The new distortion solution, in the form of two FITS files, may be obtained at http://www.astro.ucla.edu/∼ghezgroup/distortion or by emailing the first author. The FITS files, or look-up tables, may be fed into the IRAF routine *Drizzle* during the data reduction process. The values in the look-up tables specify the shifts required to put an image in a "distortion-free" reference frame. The errors in the distortion solutions may also be obtained at this site.

We thank the staff of the Keck Observatory, especially Randy Campbell, Al Conrad, Jim Lyke, and Hien Tran for their help in obtaining the observations. We also thank Tuan Do, Quinn Konopacky and Kieth Matthews for their helpful suggestions on this work and the manuscript. Support for this work was provided by the NSF grant AST-0406816 and the NSF Science & Technology Center for Adaptive Optics, managed by UCSC (AST-9876783). The W. M. Keck Observatory is operated as a scientific partnership among the California Institute of Technology, the University of California and the National Aeronautics and Space Administration. The Observatory was made possible by the generous financial support of the W. M. Keck Foundation.

Facilities: Keck: II (NIRC2)

REFERENCES

Anderson, J. 2005, in The 2005 HST Calibration Workshop Proceedings, ed. A. Koekemoer, P. Goudfrooij, & L. L. Dressel, 11–20

Anderson, J. 2007, Variation of the Distortion Solution, Tech. rep.

Anderson, J., & King, I. R. 2003, PASP, 115, 113

—. 2006, PSFs, Photometry, and Astronomy for the ACS/WFC, Tech. rep.

Anderson, J., Sarajedini, A., Bedin, L. R., King, I. R., Piotto, G., Reid, I. N., Siegel, M., Majewski, S. R., Paust, N. E. Q., Aparicio, A., Milone, A. P., Chaboyer, B., & Rosenberg, A. 2008, AJ, 135, 2055

Cameron, P. B., & Kulkarni, S. R. 2007, in Bulletin of the American Astronomical Society, Vol. 38, Bulletin of the American Astronomical Society, 996–+

Dierckx, P. 1995, Curve and Surface Fitting with Splines (Oxford University Press)

Diolaiti, E., Bendinelli, O., Bonaccini, D., Close, L., Currie, D., & Parmeggiani, G. 2000, A&AS, 147, 335

Do, T., Ghez, A. M., Morris, M. R., Lu, J. R., Matthews, K., Yelda, S., & Larkin, J. 2009, ArXiv e-prints

Dupuy, T. J., Liu, M. C., & Ireland, M. J. 2008, ArXiv e-prints

Eckart, A., & Genzel, R. 1997, MNRAS, 284, 576

Fragile, P. C., & Mathews, G. J. 2000, ApJ, 542, 328

Fruchter, A. S., & Hook, R. N. 2002, PASP, 114, 144

Genzel, R., Pichon, C., Eckart, A., Gerhard, O. E., & Ott, T. 2000, MNRAS, 317, 348

Genzel, R., Schödel, R., Ott, T., Eisenhauer, F., Hofmann, R., Lehnert, M., Eckart, A., Alexander, T., Sternberg, A., Lenzen, R., Clénet, Y., Lacombe, F., Rouan, D., Renzini, A., & Tacconi-Garman, L. E. 2003, ApJ, 594, 812

Ghez, A. M., Klein, B. L., Morris, M., & Becklin, E. E. 1998, ApJ, 509, 678

Ghez, A. M., Salim, S., Weinberg, N. N., Lu, J. R., Do, T., Dunn, J. K., Matthews, K., Morris, M., Yelda, S., Becklin, E. E., Kremenek, T., Milosavljevic, M., & Naiman, J. 2008, ApJ, In press

Gillessen, S., Eisenhauer, F., Trippe, S., Alexander, T., Genzel, R., Martins, F., & Ott, T. 2009, ApJ, 692, 1075

Gubler, J., & Tytler, D. 1998, PASP, 110, 738

Jaroszyński, M. 1998, Acta Astronomica, 48, 413

—. 1999, ApJ, 521, 591

Konopacky, Q. M., Ghez, A. M., Duchêne, G., McCabe, C., & Macintosh, B. A. 2007, AJ, 133, 2008

Kraniotis, G. V. 2007, ArXiv e-prints

Lazorenko, P. F. 2006, AAP, 449, 1271

Lazorenko, P. F., Mayor, M., Dominik, M., Pepe, F., Segransan, D., & Udry, S. 2007, AAP, 471, 1057

Levin, Y., & Beloborodov, A. M. 2003, ApJL, 590, L33

Liu, M. C., Dupuy, T. J., & Ireland, M. J. 2008, ApJ, 689, 436

Lu, J. R. 2008, Ph.D. Thesis

Lu, J. R., Ghez, A. M., Hornstein, S. D., Morris, M. R., Becklin, E. E., & Matthews, K. 2009, ApJ, 690, 1463

Marois, C., Macintosh, B., Barman, T., Zuckerman, B., Song, I., Patience, J., Lafrenière, D., & Doyon, R. 2008, Science, 322, 1348

Nucita, A. A., De Paolis, F., Ingrosso, G., Qadir, A., & Zakharov, A. F. 2007, PASP, 119, 349

Paumard, T., Genzel, R., Martins, F., Nayakshin, S., Beloborodov, A. M., Levin, Y., Trippe, S., Eisenhauer, F., Ott, T., Gillessen, S., Abuter, R., Cuadra, J., Alexander, T., & Sternberg, A. 2006, ApJ, 643, 1011

Reid, M. J., Menten, K. M., Genzel, R., Ott, T., Schödel, R., & Eckart, A. 2003, ApJ, 587, 208

Reid, M. J., Menten, K. M., Trippe, S., Ott, T., & Genzel, R. 2007, ApJ, 659, 378

Rubilar, G. F., & Eckart, A. 2001, AAP, 374, 95

Salim, S., & Gould, A. 1999, ApJ, 523, 633

Stolte, A., Ghez, A. M., Morris, M., Lu, J. R., Brandner, W., & Matthews, K. 2008, ApJ, 675, 1278

van der Marel, R. P., Anderson, J., Cox, C., Kozhurina-Platais, V., Lallo, M., & Nelan, E. 2007, Calibration of ACS/WFC Absolute Scale and Rotation for Use in creation of a JWST Astrometric Reference Field, Tech. rep.

Weinberg, N. N., Milosavljević, M., & Ghez, A. M. 2005, ApJ, 622, 878

Will, C. M. 2008, ApJL, 674, L25

Zucker, S., & Alexander, T. 2007, ApJL, 654, L83

This preprint was prepared with the AAS LaTeX macros v5.2.

A. Differential Atmospheric Refraction

A pair of stars viewed through the Earth's atmosphere will have different separations depending on the zenith angle at which they are viewed. This effect is due to differential atmospheric refraction (DAR) and is described in detail in Gubler & Tytler (1998), Lazorenko (2006), and Lazorenko et al. (2007)[4]. There is both chromatic and achromatic differential atmospheric refraction; however, the achromatic term is at least 20 times larger than the chromatic term (Gubler & Tytler 1998). Sources at the Galactic center have similar colors due to the high extinction and, as a result, the chromatic term is negligible. Color differences for stars in M92, however, may result in small residual systematic errors ($\sim$0.2 mas) in our comparison of ground-based to space-based astrometry due to chromatic DAR, but this effect is smaller than the residual distortion in ACS/WFC ($\sim$0.5 mas). Therefore, the stellar positions in this work are only corrected for achromatic DAR.

The true angular separation of two stars along the zenith direction, $\Delta z = z_1 - z_2$, is modified by differential atmospheric refraction such that the observed angular separation becomes $\Delta z_{obs} = \Delta z_{true} - \Delta R$. Neglecting chromatic effects, the DAR term (ΔR) depends only on (1) the observed zenith angle of star 1, (2) the wavelength of the observations, (3) the observed zenith separation of star 1 and star 2, (4) the temperature at the observatory, (5) the pressure at the observatory, and (6) the relative humidity at the observatory. The atmospheric parameters of interest are downloaded from an archive maintained at the Canada-France-Hawaii Telescope (CFHT)[5]. These values are recorded every five minutes, allowing us to find the appropriate atmospheric conditions on Mauna Kea within three minutes of the observation (Lu 2008). During our observations, the typical atmospheric conditions at night on Mauna Kea have a temperature of 272 K, a relative humidity of 10%, and a pressure of 617 millibars. Figure 4 shows, for these typical conditions, the magnitude of DAR. We also show the actual magnitude of the effect for the individual images as points along the 10" case, showing that the variations in conditions do not have a significant effect on DAR.

[4]See also Evans, D. W., "Atmospheric Differential Refraction in the Infrared", 2004, `http://www.ast.cam.ac.uk/vdfs/documentation.html`

[5]`http://kiloaoloa.soest.hawaii.edu/archive/wx/cfht/`

Table 1. Summary of M92 Images

Date[a] (UT)	PA	$(X,Y)_{GS}$[b] (pix)	$\Delta(X,Y)$[c] (pix)	El (deg)	Temp (K)	Pressure (mbar)	RH[d] %	ΔR[e] (mas)	$t_{exp,i} \times$coadd (sec)	$\langle$FWHM$\rangle$ (mas)	$\langle$Strehl$\rangle$	N stars detected	N stars used	$\langle\sigma_{pos}\rangle$[f] (pix)
2007 June 21	0	508, 512	0, 0	53	271.2	616.8	92	2.74	3.0×10	49	0.55	105	69	0.037
			254, -252	53	271.1	616.7	89	2.77		48	0.55	145	58	0.035
			251, 252	52	271.1	616.7	89	2.81		48	0.57	112	46	0.045
			-251, -252	52	271.3	616.7	93	2.84		48	0.59	176	56	0.034
			-253, 250	51	271.3	616.7	93	2.89		49	0.54	110	57	0.037
			251, 0	51	271.2	616.7	95	2.93		48	0.60	124	58	0.044
			-251, -1	50	271.2	616.7	95	2.97		47	0.59	115	64	0.049
			2, -250	50	271.1	616.7	96	3.02		47	0.58	124	47	0.063
			0, 253	49	271.0	616.6	97	3.07		46	0.61	94	51	0.058
2007 July 29	90	457, 499	0, 0	67	272.9	615.3	11	2.07	0.8×60	45	0.64	73	47	0.031
			255, -251	67	272.9	615.3	11	2.07		45	0.72	53	38	0.048
			251, 255	67	272.9	615.3	12	2.07		45	0.68	84	41	0.042
			-249, -251	67	272.9	615.2	12	2.07		46	0.66	65	40	0.052
			-252, 251	67	272.9	615.2	13	2.07		45	0.69	132	52	0.031
			254, 2	67	272.9	615.3	13	2.07		45	0.71	72	44	0.021
			-252, 0	66	272.9	615.2	13	2.08		45	0.72	93	48	0.037
			3, -250	66	272.8	615.2	12	2.09		44	0.73	69	47	0.029
			-2, 253	66	272.8	615.2	12	2.10		45	0.72	92	51	0.024
			-125, -124	65	272.8	615.2	12	2.11		45	0.72	85	50	0.026
			128, -375	65	272.8	615.2	13	2.12		45	0.73	89	48	0.030
			126, 129	65	272.8	615.2	12	2.14		45	0.70	84	54	0.030
			-374, -376	64	272.8	615.2	13	2.16		46	0.69	47	33	0.033
			-378, 126	64	272.8	615.2	12	2.18		46	0.68	74	39	0.067
			128, -123	63	272.9	615.2	12	2.20		46	0.67	77	49	0.038
			-374, -125	62	272.9	615.2	12	2.22		46	0.67	72	38	0.032
			-121, -374	62	272.9	615.2	12	2.25		46	0.67	51	38	0.028
			-127, 129	61	273.0	615.2	11	2.27		46	0.66	87	45	0.045
			127, -121	60	273.1	615.1	11	2.31		46	0.65	81	47	0.045
			380, -373	60	273.2	615.1	12	2.34		47	0.63	52	33	0.071
			378, 132	59	273.1	615.1	12	2.38		46	0.65	51	39	0.025
			-126, -373	58	273.3	615.1	12	2.41		46	0.66	54	36	0.032
			-128, 130	57	273.3	615.1	11	2.46		47	0.65	76	45	0.031
			381, -120	56	273.3	615.0	11	2.50		47	0.64	43	35	0.040

Table 1—Continued

Date[a] (UT)	PA	$(X,Y)_{GS}$[b] (pix)	$\Delta(X,Y)$[c] (pix)	El (deg)	Temp (K)	Pressure (mbar)	RH[d] %	ΔR[e] (mas)	$t_{exp,i} \times$coadd (sec)	$\langle$FWHM$\rangle$ (mas)	$\langle$Strehl$\rangle$	N stars detected	N stars used	$\langle\sigma_{pos}\rangle$[f] (pix)
			-127, -120	56	273.4	615.0	10	2.55		47	0.61	64	43	0.022
			129, -371	55	273.3	615.0	12	2.60		47	0.63	54	39	0.040
			124, 133	54	273.3	614.9	11	2.66		48	0.60	79	47	0.036
2008 Apr 28	180	496, 477	0, 0	67	271.0	615.8	82	2.08	0.8×60	47	0.56	31	20	0.022
			252, -252	67	271.0	615.7	81	2.08		48	0.53	32	0	-1.000
			248, 253	67	271.0	615.8	83	2.08		48	0.55	55	15	0.061
			113, -375	63	271.5	616.0	70	2.23		48	0.54	12	0	-1.000
			-143, -120	59	271.0	616.0	77	2.39		51	0.44	13	9	0.022
2008 June 3	0	776, 573	0, 0	42	273.3	616.0	64	3.85	1.5×6	50	0.47	30	0	-1.000
			4, 4	42	273.2	616.1	65	3.89		51	0.48	32	0	-1.000
			-4, 0	42	273.2	616.1	65	3.93		58	0.29	29	0	-1.000
			4, 0	41	273.2	616.1	65	3.97		54	0.38	32	0	-1.000
			-4, 3	41	273.2	616.1	65	4.01		54	0.38	25	0	-1.000
			-5, -4	41	273.2	616.1	65	4.05		54	0.40	26	0	-1.000
2008 July 24	45	173, 565	0, 0	50	271.6	617.2	39	3.03	2.8×10	66	0.35	128	32	0.077
			0, -49	49	271.6	617.2	39	3.07		63	0.35	110	35	0.068
			0, -100	49	271.6	617.1	39	3.11		72	0.30	88	30	0.065
			1, -149	48	271.6	617.1	39	3.16		72	0.29	89	30	0.089
			3, -199	48	271.6	616.9	39	3.21		51	0.46	131	45	0.065
			2, -249	47	271.6	616.9	39	3.26		86	0.22	89	21	0.067
2009 May 9	0	910, 668	0, 0	66	270.6	614.6	36	2.11	0.8×60	52	0.45	18	10	0.072
			1, -153	66	270.6	614.6	36	2.12		49	0.50	19	15	0.031
			3, -304	65	270.6	614.6	36	2.13		49	0.47	19	16	0.026
			-154, -2	65	270.5	614.6	36	2.14		51	0.48	25	17	0.036
			-153, -154	65	270.5	614.7	36	2.15		47	0.58	30	25	0.036
			-152, -305	64	270.5	614.7	36	2.16		50	0.47	27	22	0.038
			-305, -4	64	270.8	614.7	35	2.17		50	0.51	23	19	0.034
			-305, -155	64	271.0	614.7	35	2.18		56	0.38	26	12	0.041
			-302, -306	63	271.0	614.7	35	2.20		63	0.30	22	13	0.033

Table 1—Continued

Date[a] (UT)	PA	$(X,Y)_{GS}$[b] (pix)	$\Delta(X,Y)$[c] (pix)	El (deg)	Temp (K)	Pressure (mbar)	RH[d] %	ΔR[e] (mas)	$t_{exp,i} \times$coadd (sec)	$\langle$FWHM$\rangle$ (mas)	$\langle$Strehl$\rangle$	N stars detected	N stars used	$\langle\sigma_{pos}\rangle$[f] (pix)
2009 May 9	90	365, 411	0, 0	62	270.8	614.6	35	2.27	0.8×60	49	0.49	25	19	0.025
			2, -153	61	270.8	614.6	35	2.29		50	0.48	24	17	0.028
			0, -302	61	270.8	614.5	35	2.31		50	0.47	10	8	0.031
			-151, -1	60	270.8	614.5	35	2.33		50	0.48	28	19	0.061
			-152, -154	60	270.8	614.5	36	2.35		47	0.56	29	22	0.035
			-149, -304	59	270.8	614.5	36	2.37		46	0.67	26	20	0.020
			-302, -4	59	270.6	614.5	36	2.40		46	0.61	35	24	0.023
			-304, -156	58	270.7	614.5	34	2.42		46	0.64	29	26	0.025
			-301, -305	58	270.7	614.5	34	2.45		48	0.53	18	15	0.030
2009 May 9	315	697, 499	0, 0	56	271.1	614.5	33	2.55	0.8×60	45	0.67	38	27	0.055
			2, -152	55	271.1	614.5	33	2.58		45	0.68	48	29	0.055
			0, -304	55	271.0	614.4	34	2.62		45	0.67	58	30	0.060
			-152, 0	54	270.7	614.3	35	2.66		47	0.56	35	22	0.044
			-148, -154	54	270.7	614.3	35	2.69		56	0.32	21	13	0.085
			-149, -305	53	270.7	614.3	35	2.74		50	0.45	43	18	0.078
			-300, -2	53	270.6	614.4	35	2.78		50	0.45	25	18	0.044
			-301, -154	52	270.6	614.5	35	2.82		59	0.29	21	13	0.063

[a]2008 June 3 data set taken in LGS-AO mode. All other data sets taken with NGS-AO.

[b]Position of guide star in first image of a given epoch.

[c]Positional offset of guide star in NIRC2 pixels relative to first pointing of epoch.

[d]Relative Humidity.

[e]Differential Atmospheric Refraction over 10".

[f]Images thrown out are given a value of -1.0 for the average positional uncertainty.

Table 2. Maser Astrometric Errors

Star Name	[IR − Radio] Position X (mas)	Y (mas)	Total (mas)	Error in IR[a] Centroid (mas)	Error in Radio Position (mas)	Error in Alignment (mas)	ΔR[b] (mas)
IRS 9	-1.92	0.80	2.13	1.90	0.78	0.66	-2.27
IRS 7	2.44	-7.80	8.19	1.60	5.30	0.71	2.24
IRS 12N	-2.58	-3.26	4.41	3.86	1.30	0.95	-2.98
IRS 28	-3.42	3.80	5.29	2.42	1.50	0.67	-1.81
IRS 10EE	-0.50	2.24	2.35	1.62	0.58	0.57	2.11
IRS 15NE	0.76	3.36	3.64	1.64	0.86	0.85	4.64
IRS 17	2.72	0.76	2.96	1.62	3.76	0.74	2.95

[a]Error in IR centroid includes distortion error and residual distortion

[b]Differential Atmospheric Refraction

Table 3. NIRC2 Plate Scale and Orientation

Method	Plate Scale (mas/pix)	Orientation (deg)
Calibrated w.r.t. ACS observations of M92	$9.948 \pm 0.001 \pm 0.001$	$0.256 \pm 0.006 \pm 0.001$
Calibrated w.r.t. VLA observations of GC Masers	9.953 ± 0.001	0.256 ± 0.003
Final Value	9.951 ± 0.002	0.256 ± 0.007

Note. — Statistical and absolute uncertainties are shown for the ACS observations.

Table 4. Absolute Astrometry of Known Late Type Stars in the Galactic Center

Name	K (mag)	Epoch (year)	Radius (arcsec)	Δ R.A.[a] (arcsec)	Δ Decl.[a] (arcsec)	v_x (mas/yr)	v_y (mas/yr)	Ref[b]
S0-12	14.3	2007.49	0.688	-0.555	0.406	0.5 ± 1.2	3.5 ± 1.2	1
S0-13	13.5	2007.30	0.692	0.550	-0.419	1.8 ± 0.5	3.1 ± 0.6	1
S1-10	14.9	2007.33	1.112	-1.112	-0.020	4.0 ± 0.6	2.2 ± 0.6	1
S1-13	14.1	2007.68	1.485	-1.136	-0.956	-3.4 ± 0.7	-7.5 ± 0.7	1
S1-15	14.0	2007.74	1.445	-1.356	0.499	-0.7 ± 1.0	-3.2 ± 1.1	1
S1-17	12.4	2007.33	1.586	0.476	-1.513	-0.1 ± 0.5	-5.7 ± 0.6	1
S1-20	12.7	2007.32	1.661	0.432	1.604	4.1 ± 0.5	0.0 ± 0.6	1
S1-23	11.7	2007.70	1.746	-0.908	-1.491	4.2 ± 0.7	-3.9 ± 0.7	1
S1-25	13.4	2007.34	1.777	1.666	-0.617	3.2 ± 0.5	2.7 ± 0.6	1
S1-5	12.7	2007.33	0.957	0.327	-0.899	-3.9 ± 0.5	4.2 ± 0.6	1
S1-68	13.4	2007.37	1.951	1.844	-0.637	-5.0 ± 0.6	-5.5 ± 0.6	1
S2-11	12.0	2007.31	2.063	1.970	-0.613	-0.9 ± 0.5	1.7 ± 0.6	1
S2-18	13.2	2007.33	2.362	-0.994	-2.143	-2.9 ± 0.6	-1.9 ± 0.6	1
S2-19	12.5	2007.31	2.338	0.401	2.304	-8.2 ± 0.6	1.3 ± 0.6	2
S2-2	13.9	2007.30	2.145	-0.530	2.079	2.3 ± 0.6	5.0 ± 0.7	1
S2-23	14.5	2007.31	2.406	1.651	1.750	-1.1 ± 0.5	-1.9 ± 0.6	1
S2-25	13.8	2007.40	2.547	0.751	-2.433	2.7 ± 0.6	3.3 ± 0.6	1
S2-26	13.8	2007.34	2.475	0.773	2.351	5.0 ± 0.6	-13.7 ± 0.7	1
S2-3	14.3	2006.88	2.081	-1.531	-1.409	1.5 ± 0.8	-2.7 ± 0.8	1
S2-31	13.1	2007.37	2.786	2.779	-0.196	-6.9 ± 0.5	1.3 ± 0.6	1
S2-32	12.2	2007.24	2.999	1.125	2.780	-0.3 ± 0.5	1.9 ± 0.6	1
S2-47	14.3	2007.43	2.255	2.194	-0.521	0.2 ± 0.6	1.8 ± 0.6	1
S2-57	14.4	2007.52	2.404	-1.174	-2.098	8.7 ± 0.7	4.3 ± 0.7	1
S2-67	13.5	2007.26	2.628	-2.482	-0.866	3.0 ± 0.6	-6.3 ± 0.6	2
S2-69	14.7	2007.53	2.690	-0.878	2.542	-1.7 ± 0.7	5.4 ± 0.7	2
S2-70	14.4	2007.53	2.692	-2.662	0.401	-6.2 ± 0.9	-1.9 ± 0.9	1
S2-72	14.9	2007.55	2.699	-1.480	-2.257	-6.9 ± 0.7	6.8 ± 0.7	1
S2-75	14.5	2007.34	2.773	2.635	-0.865	-0.4 ± 0.5	4.8 ± 0.6	1
S2-78	13.6	2007.69	2.828	-2.814	-0.284	-2.0 ± 0.7	0.6 ± 0.8	2
S2-8	12.1	2007.70	2.152	-1.963	0.882	2.0 ± 0.7	2.7 ± 0.8	1
S2-85	12.4	2007.23	2.972	-1.278	2.683	-5.5 ± 0.5	-2.8 ± 0.6	2
S3-136	14.5	2007.41	3.337	-3.019	-1.420	-3.8 ± 0.7	0.3 ± 0.7	2
S3-14	13.8	2007.26	3.083	0.139	3.079	13.2 ± 0.5	-3.2 ± 0.6	1
S3-187	14.4	2007.60	3.480	-3.400	-0.745	-1.7 ± 0.7	-0.3 ± 0.7	2
S3-198	13.6	2007.29	3.516	0.651	3.455	-0.3 ± 0.5	-1.1 ± 0.6	2
S3-20	14.6	2007.46	3.207	1.584	-2.789	-0.7 ± 0.6	0.6 ± 0.6	1
S3-207	13.9	2007.42	3.555	1.541	3.204	2.7 ± 0.6	3.0 ± 0.6	2
S3-22	11.2	2007.58	3.226	-0.349	-3.208	3.1 ± 0.7	-1.8 ± 0.7	2
S3-249	14.4	2007.82	3.623	-3.381	1.301	0.5 ± 0.7	-7.5 ± 0.8	1
S3-27	14.1	2007.29	3.355	-0.324	3.340	-1.6 ± 0.5	-5.8 ± 0.6	2
S3-284	13.6	2007.31	3.739	-2.574	2.712	1.3 ± 0.6	0.5 ± 0.6	2
S3-288	14.1	2007.25	3.754	-2.767	2.536	-3.3 ± 0.5	0.5 ± 0.6	2
S3-35	13.8	2007.42	3.508	-1.199	3.296	-4.4 ± 0.6	-3.8 ± 0.7	2
S3-36	14.7	2007.33	3.563	3.467	-0.817	1.2 ± 0.6	1.0 ± 0.6	1
S3-39	13.4	2007.57	3.726	3.563	1.089	-2.3 ± 0.6	-1.8 ± 0.7	1

Table 4—Continued

Name	K (mag)	Epoch (year)	Radius (arcsec)	Δ R.A.[a] (arcsec)	Δ Decl.[a] (arcsec)	v_x (mas/yr)	v_y (mas/yr)	Ref[b]
S3-6	12.9	2007.40	3.230	3.229	-0.030	1.4 ± 0.6	-7.4 ± 0.6	1
S3-8	13.9	2007.47	3.448	3.412	-0.497	-0.5 ± 0.6	-0.6 ± 0.6	1
S4-1	13.3	2007.55	4.029	4.013	-0.364	-4.4 ± 0.6	0.1 ± 0.6	1
S4-161	13.6	2007.53	4.420	4.412	-0.261	1.6 ± 0.6	1.9 ± 0.6	2
S4-2	12.4	2007.38	4.107	3.758	1.658	1.9 ± 0.5	-2.1 ± 0.6	1
S4-207	11.4	2007.68	4.557	-4.059	-2.072	1.1 ± 0.8	-1.5 ± 0.8	2
S4-221	14.3	2007.36	4.607	2.671	-3.754	6.8 ± 0.6	-4.5 ± 0.6	2
S4-24	13.8	2007.25	4.063	-0.730	3.996	2.2 ± 0.5	2.2 ± 0.6	2
S4-25	13.9	2007.43	4.085	2.449	3.270	1.9 ± 0.6	4.0 ± 0.6	2
S4-3	12.9	2007.47	4.212	4.210	0.121	3.9 ± 0.5	1.4 ± 0.6	2
S4-342	14.0	2007.40	4.938	3.063	3.873	0.9 ± 0.6	-2.9 ± 0.6	2
S4-4	11.9	2007.50	4.340	3.600	-2.424	2.1 ± 0.6	-6.2 ± 0.6	2
S4-46	14.7	2007.57	4.122	3.846	-1.484	-1.4 ± 0.6	1.9 ± 0.6	2
S4-59	13.6	2007.21	4.121	-3.161	2.644	1.8 ± 0.6	0.8 ± 0.6	2
S4-6	12.8	2007.42	4.272	3.276	-2.742	2.5 ± 0.6	-3.1 ± 0.6	2
S5-168	14.1	2007.43	5.680	4.378	3.619	-2.3 ± 0.6	0.0 ± 0.6	2
S5-170	14.0	2007.61	5.707	4.219	3.843	2.8 ± 0.6	-2.6 ± 0.7	2
S5-215	10.5	2006.60	5.978	-3.695	-4.698	-1.4 ± 1.0	-4.7 ± 1.0	2
S5-34	13.8	2007.53	5.121	-4.328	-2.737	-3.6 ± 1.1	-3.0 ± 1.1	2
S5-47	13.2	2007.25	5.160	2.867	4.290	0.3 ± 0.5	5.4 ± 0.6	2
S5-83	14.6	2007.52	5.293	5.211	-0.930	-3.2 ± 0.6	-6.3 ± 0.6	2
S5-92	13.5	2007.35	5.336	4.291	3.171	-2.1 ± 0.6	-2.8 ± 0.6	2
S6-24	14.3	2007.47	6.222	5.084	3.588	3.5 ± 0.6	2.1 ± 0.6	2
S6-67	13.5	2007.50	6.644	5.050	4.317	-5.8 ± 0.6	2.1 ± 0.6	2
S6-71	14.9	2007.68	6.800	5.260	4.309	-3.8 ± 0.6	2.5 ± 0.7	2
S6-83	10.5	2007.39	6.969	6.912	0.897	2.1 ± 0.5	-2.3 ± 0.5	2
S6-84	10.9	2007.44	6.967	6.964	-0.200	0.8 ± 0.5	-2.8 ± 0.5	2
S6-85	12.3	2007.39	6.390	6.225	-1.445	3.0 ± 0.5	3.8 ± 0.5	2
S6-86	12.4	2007.35	6.169	5.765	2.195	-1.5 ± 0.6	-4.3 ± 0.6	2
S7-8	10.4	2007.39	7.285	7.045	1.855	3.9 ± 0.5	1.0 ± 0.5	2
irs15SW	10.7	2007.21	11.718	-0.613	11.702	-3.1 ± 0.7	1.7 ± 0.8	2
irs1NE	10.9	2007.42	7.833	7.674	1.570	-0.8 ± 0.5	-3.6 ± 0.5	2
irs1SE	10.6	2007.41	7.527	7.515	-0.434	1.9 ± 0.5	2.2 ± 0.5	2
irs29S	11.2	2007.72	2.076	-1.841	0.960	0.3 ± 0.7	0.6 ± 0.8	1
irs7	7.4	2007.22	5.523	0.034	5.522	-0.5 ± 0.5	-4.2 ± 0.6	2
-	12.0	2007.22	8.114	3.676	7.234	3.3 ± 0.5	4.1 ± 0.6	2
-	12.1	2007.13	11.913	4.483	11.038	-2.1 ± 0.5	1.8 ± 0.6	2
-	12.3	2007.55	11.454	9.482	6.425	2.1 ± 0.8	-0.1 ± 0.9	2
-	12.3	2007.23	4.917	1.455	4.697	-1.0 ± 0.5	5.0 ± 0.6	2
-	12.5	2007.28	6.977	3.040	6.280	3.3 ± 0.6	3.3 ± 0.7	2
-	12.6	2007.32	8.362	7.973	2.521	0.8 ± 0.6	2.3 ± 0.6	2
-	12.6	2007.14	7.506	1.003	7.439	1.8 ± 0.5	2.1 ± 0.6	2
-	12.7	2007.22	4.851	-0.860	4.774	-1.2 ± 0.5	-1.8 ± 0.6	2
-	12.7	2007.32	11.539	8.156	8.162	-0.5 ± 0.5	0.6 ± 0.6	2
-	12.6	2007.44	5.740	5.711	0.575	-1.6 ± 0.5	-4.5 ± 0.6	2

Table 4—Continued

Name	K (mag)	Epoch (year)	Radius (arcsec)	Δ R.A.[a] (arcsec)	Δ Decl.[a] (arcsec)	v_x (mas/yr)	v_y (mas/yr)	Ref[b]
-	13.0	2007.15	6.213	-2.986	5.448	-2.9 ± 0.5	-0.6 ± 0.6	2
-	10.6	2007.08	8.764	-2.260	8.467	-3.5 ± 0.5	4.0 ± 0.7	2
-	13.1	2007.11	11.685	0.025	11.685	-2.1 ± 0.5	-0.8 ± 0.7	2
-	13.3	2007.31	9.157	5.963	6.950	4.5 ± 0.5	1.2 ± 0.6	2
-	13.2	2007.27	8.931	3.572	8.186	-2.0 ± 0.5	2.7 ± 0.6	2
-	10.7	2007.37	9.538	8.599	4.127	4.0 ± 0.5	0.9 ± 0.6	2
-	13.3	2007.39	9.650	8.401	4.749	0.1 ± 0.5	-3.3 ± 0.6	2
-	13.3	2007.13	10.384	1.430	10.285	-4.8 ± 0.5	5.5 ± 0.7	2
-	13.2	2007.19	4.753	1.332	4.563	-3.1 ± 0.5	-0.6 ± 0.6	2
-	13.5	2007.42	10.219	5.534	8.591	1.5 ± 0.6	-2.5 ± 0.7	2
-	13.4	2007.39	9.985	9.036	4.248	-0.5 ± 0.5	3.1 ± 0.6	2
-	13.5	2007.48	10.167	9.695	3.063	4.3 ± 0.6	-4.0 ± 0.5	2
-	13.7	2007.46	7.379	6.242	-3.937	3.6 ± 0.6	-1.3 ± 0.6	2
-	13.6	2007.24	10.262	3.559	9.625	-1.9 ± 0.5	1.9 ± 0.7	2
-	13.6	2007.23	7.570	2.723	7.063	-7.3 ± 0.5	-4.8 ± 0.6	2
-	13.5	2007.33	6.911	5.112	4.650	1.5 ± 0.5	-3.7 ± 0.6	2
-	13.7	2007.58	10.339	10.336	-0.255	2.1 ± 0.6	-5.4 ± 0.6	2
-	13.7	2007.44	7.923	7.406	2.816	-7.2 ± 0.6	3.5 ± 0.6	2
-	13.7	2007.12	8.574	-1.135	8.498	-3.9 ± 0.5	1.1 ± 0.7	2
-	13.7	2007.28	11.864	8.839	7.914	1.9 ± 0.6	0.2 ± 0.6	2
-	14.0	2007.51	15.513	10.237	11.655	-0.7 ± 0.7	4.2 ± 0.7	2
-	13.7	2007.37	6.533	4.526	4.712	1.4 ± 0.5	0.1 ± 0.6	2
-	13.9	2007.28	12.091	5.809	10.604	1.9 ± 0.6	4.1 ± 0.7	2
-	13.9	2007.25	9.917	7.448	6.548	0.1 ± 0.6	0.8 ± 0.6	2
-	13.9	2007.35	10.186	8.510	5.598	2.4 ± 0.5	-2.4 ± 0.6	2
-	13.9	2007.31	9.995	6.385	7.689	-1.5 ± 0.6	1.2 ± 0.6	2
-	13.8	2007.23	9.990	4.311	9.011	-5.9 ± 0.5	2.2 ± 0.6	2
-	14.0	2007.27	12.543	10.483	6.886	0.8 ± 0.6	0.7 ± 0.6	2
-	13.8	2007.55	6.924	6.686	1.800	-2.7 ± 0.6	0.8 ± 0.6	2
-	14.0	2007.17	8.530	-3.577	7.743	0.8 ± 0.6	3.3 ± 0.7	2
-	14.0	2007.16	6.694	-5.686	3.532	-2.1 ± 0.6	0.2 ± 0.7	2
-	13.8	2007.28	12.841	5.469	11.618	2.7 ± 0.6	2.7 ± 0.7	2
-	14.0	2007.34	12.113	9.001	8.106	2.3 ± 0.6	1.2 ± 0.6	2
-	14.1	2007.11	10.123	0.372	10.117	-3.1 ± 0.5	1.2 ± 0.7	2
-	14.0	2007.31	8.835	2.983	8.316	-3.3 ± 0.5	0.4 ± 0.6	2
-	14.0	2007.51	6.840	6.701	1.375	1.8 ± 0.6	2.7 ± 0.6	2
-	14.2	2007.25	12.758	5.917	11.303	-0.6 ± 0.6	4.2 ± 0.7	2
-	13.9	2007.33	9.014	3.905	8.124	-0.2 ± 0.6	-6.0 ± 0.7	2
-	14.1	2007.32	8.809	6.893	5.485	-1.2 ± 0.5	3.0 ± 0.6	2
-	14.2	2007.42	7.280	7.274	-0.287	-1.5 ± 0.5	-5.8 ± 0.5	2
-	14.3	2007.13	11.909	-3.490	11.386	-5.0 ± 0.7	0.8 ± 0.8	2
-	14.2	2007.16	10.443	3.044	9.990	0.4 ± 0.5	3.2 ± 0.6	2
-	14.2	2007.27	11.022	6.621	8.812	1.5 ± 0.6	0.8 ± 0.6	2
-	14.1	2007.41	7.441	3.526	6.552	-0.1 ± 0.6	2.8 ± 0.7	2
-	14.0	2007.29	6.301	-1.264	6.173	-4.1 ± 0.6	0.5 ± 0.7	2

Table 4—Continued

Name	K (mag)	Epoch (year)	Radius (arcsec)	Δ R.A.[a] (arcsec)	Δ Decl.[a] (arcsec)	v_x (mas/yr)	v_y (mas/yr)	Ref[b]
-	14.3	2007.47	9.265	-0.699	9.238	-1.6 ± 0.6	-1.6 ± 0.8	2
-	14.2	2007.34	9.922	9.386	3.217	2.7 ± 0.6	-4.2 ± 0.6	2
-	14.2	2007.54	6.974	5.016	4.846	-5.5 ± 0.6	-5.7 ± 0.6	2
-	14.2	2007.21	12.076	3.408	11.585	4.9 ± 0.6	4.2 ± 0.8	2
-	14.3	2007.44	7.787	7.074	-3.256	2.4 ± 0.6	-1.8 ± 0.6	2
-	14.2	2007.52	6.357	6.304	0.823	-3.5 ± 0.6	2.7 ± 0.6	2
-	14.3	2007.27	9.753	4.003	8.894	0.8 ± 0.6	3.2 ± 0.7	2
-	14.4	2007.66	8.789	5.175	7.104	-0.5 ± 0.6	-6.3 ± 0.7	2
-	14.6	2007.37	8.281	7.370	3.776	3.8 ± 0.6	2.7 ± 0.6	2
-	14.5	2007.19	9.257	2.158	9.002	-0.2 ± 0.5	-2.9 ± 0.7	2
-	14.6	2007.57	8.475	-3.855	7.548	-3.4 ± 0.7	-2.3 ± 0.8	2
-	14.5	2007.54	6.054	6.025	-0.589	-3.7 ± 0.6	-5.2 ± 0.6	2
-	14.5	2007.36	7.273	4.755	5.504	3.0 ± 0.6	-4.8 ± 0.6	2
-	14.6	2007.59	10.027	3.946	9.218	-1.2 ± 0.6	4.3 ± 0.7	2
-	14.6	2007.21	5.735	-1.087	5.631	2.4 ± 0.6	3.0 ± 0.7	2
-	14.6	2007.48	6.963	4.220	5.538	0.7 ± 0.6	-3.1 ± 0.7	2
-	14.5	2007.32	6.698	3.023	5.977	4.4 ± 0.6	-1.5 ± 0.6	2
-	14.8	2007.39	6.968	-3.131	6.225	-3.4 ± 0.6	-4.6 ± 0.7	2
-	14.6	2007.42	7.576	3.506	6.715	-2.8 ± 0.6	2.8 ± 0.7	2
-	14.7	2007.47	12.089	11.086	4.820	1.6 ± 0.6	-3.3 ± 0.6	2
-	14.5	2007.50	11.292	7.306	8.610	-0.9 ± 0.6	0.4 ± 0.7	2
-	14.7	2007.42	9.138	7.637	5.018	-0.7 ± 0.6	1.2 ± 0.6	2
-	14.7	2007.43	8.455	5.658	6.282	1.1 ± 0.7	2.3 ± 0.7	2
-	14.8	2007.71	12.108	11.304	4.339	5.2 ± 0.6	5.7 ± 0.6	2
-	14.9	2007.48	12.568	12.299	2.588	1.3 ± 0.7	-1.1 ± 0.7	2
-	14.8	2007.56	7.856	5.993	5.079	-2.0 ± 0.6	-0.4 ± 0.6	2
-	14.9	2007.79	10.663	10.183	3.161	4.5 ± 0.7	-2.1 ± 0.6	2
-	14.9	2007.71	9.188	4.435	8.046	0.1 ± 0.7	1.8 ± 0.7	2
-	14.9	2007.45	6.931	6.708	-1.746	-3.4 ± 0.6	1.2 ± 0.6	2
-	14.9	2007.23	8.897	2.658	8.491	-2.6 ± 0.6	6.3 ± 0.7	2
-	11.7	2007.37	9.190	8.101	4.339	-1.9 ± 0.5	-2.2 ± 0.6	2
-	14.9	2007.54	8.316	1.924	8.091	6.5 ± 0.7	-1.4 ± 0.8	2
-	14.9	2007.41	8.706	2.764	8.256	-0.8 ± 0.6	2.4 ± 0.7	2
-	14.9	2007.89	9.713	9.591	1.537	2.1 ± 0.7	-0.2 ± 0.7	2
-	11.6	2007.29	6.857	4.327	5.319	-0.7 ± 0.5	-0.8 ± 0.6	2
-	11.9	2007.13	9.749	-0.547	9.733	-0.3 ± 0.5	0.7 ± 0.7	2

[a]Uncertainties in positions are typically ∼0.6 mas

[b]References for late-type identification: (1) Do et al. 2009, (2) Buchholz et al. 2009

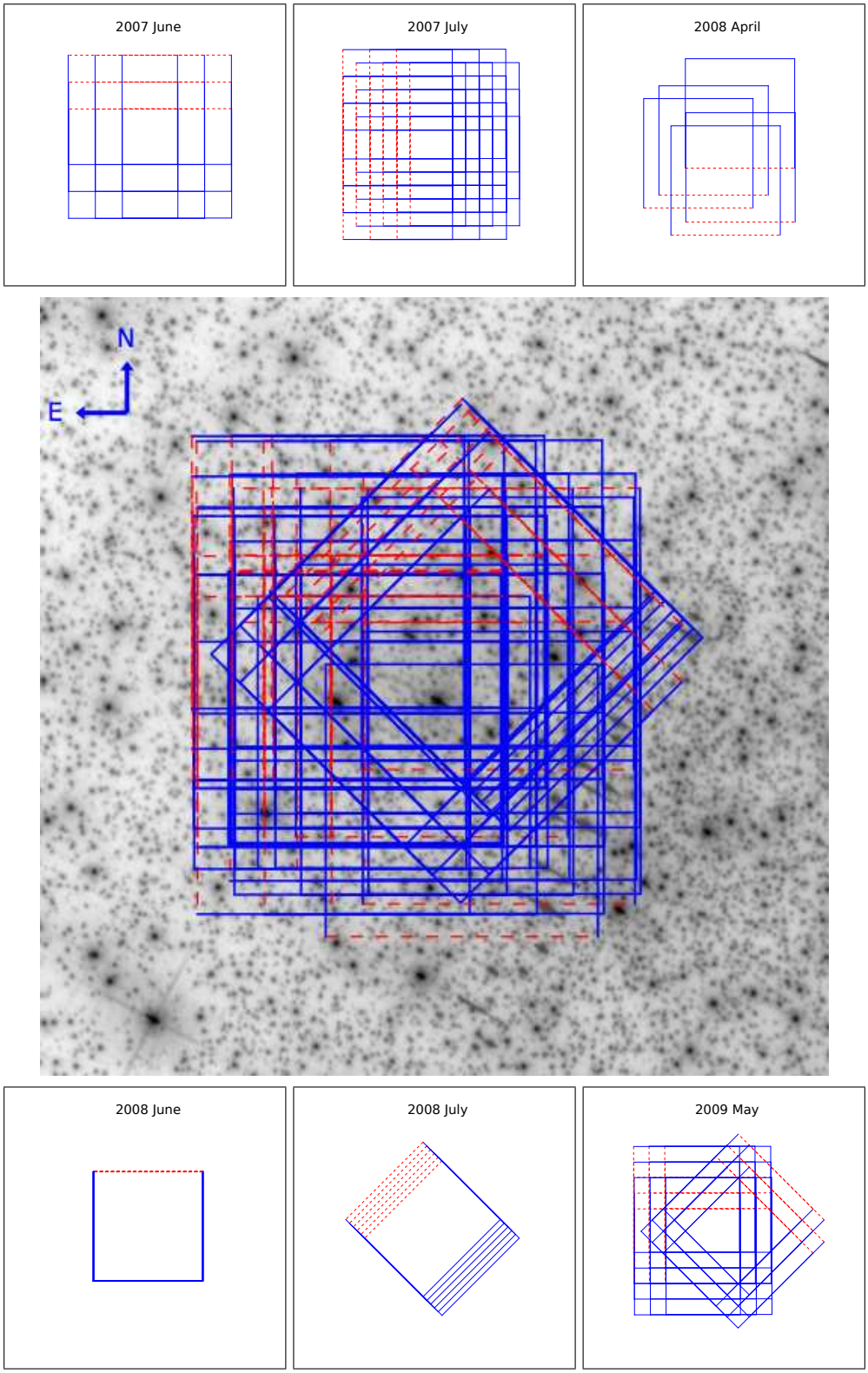

Fig. 1.— ACS/WFC image with the 79 NIRC2 pointings. The red dashed side of each NIRC2 box denotes the top of the detector's field of view. Each NIRC2 field is 10×10", while the ACS image shown is ∼30×30". The pattern for the individual epochs' exposures are shown in the insets.

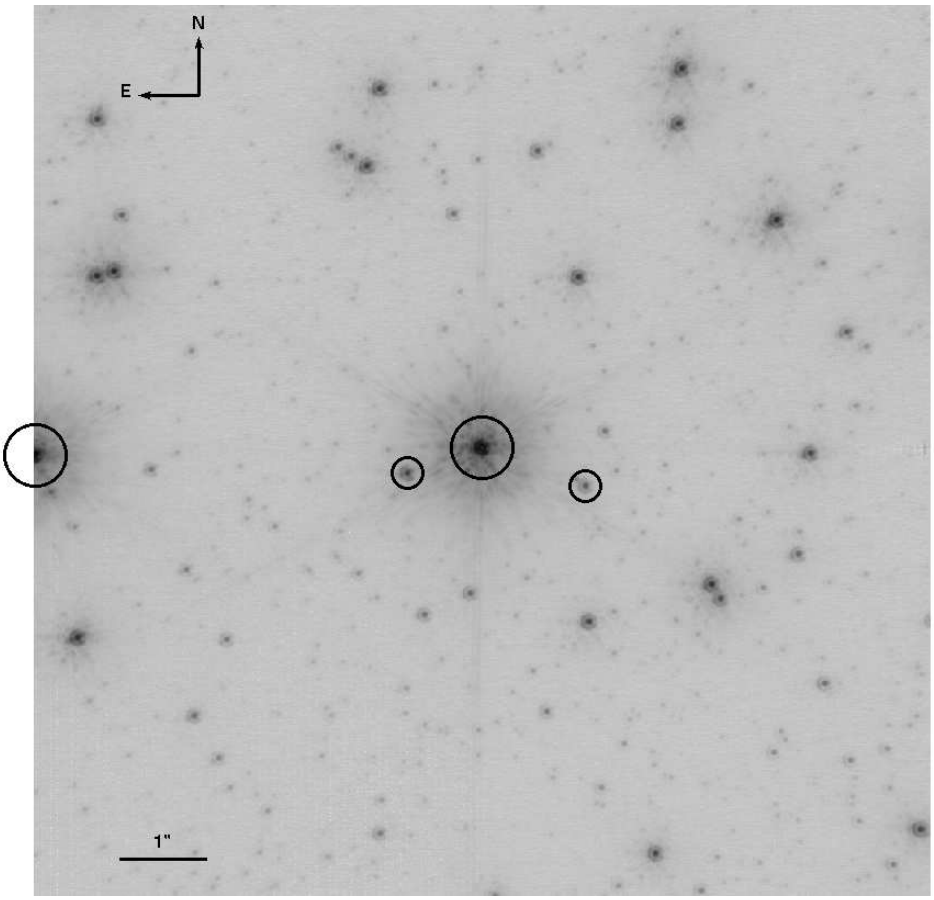

Fig. 2.— Diffraction-limited NGS-AO NIRC2 image of one of the M92 fields used to characterize the optical distortion in the NIRC2 camera. The circled stars at the center of the image, the NGS and two fainter stars, are present in most of the M92 NIRC2 observations and are used to register the images, each of which had a different position/orientation on the sky. The NGS and the circled star ∼5" to its east were almost always detected at levels that saturated the detector and were therefore removed from the analysis (see text).

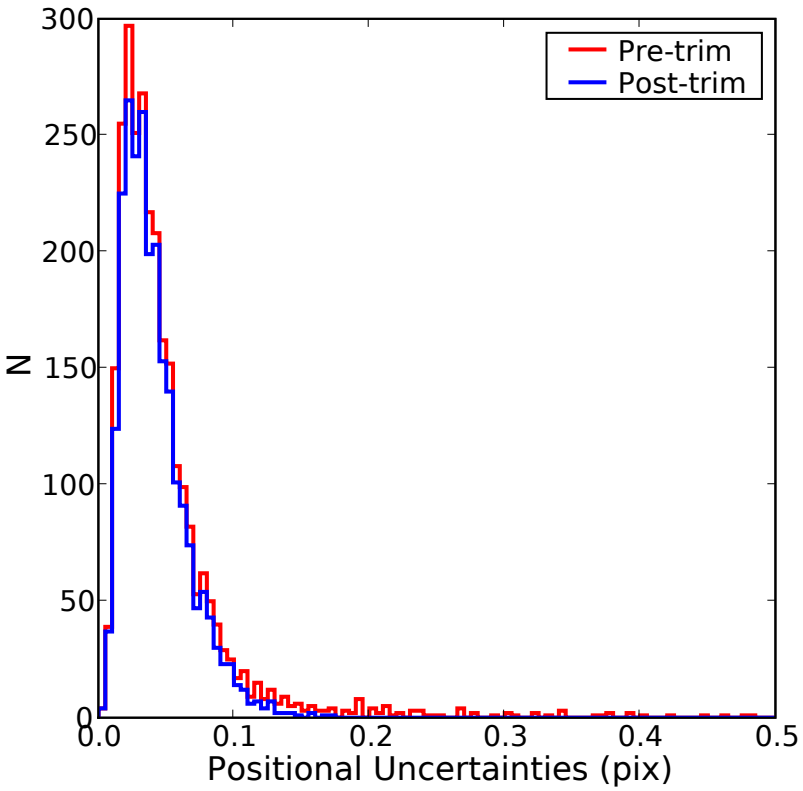

Fig. 3.— NIRC2 (plate scale ∼10 mas/pix) positional uncertainties for stars matched to the ACS/WFC star list before (*red*) and after (*blue*) removing all outliers (see text). RMS uncertainties are calculated from the three images taken at each position on the sky.

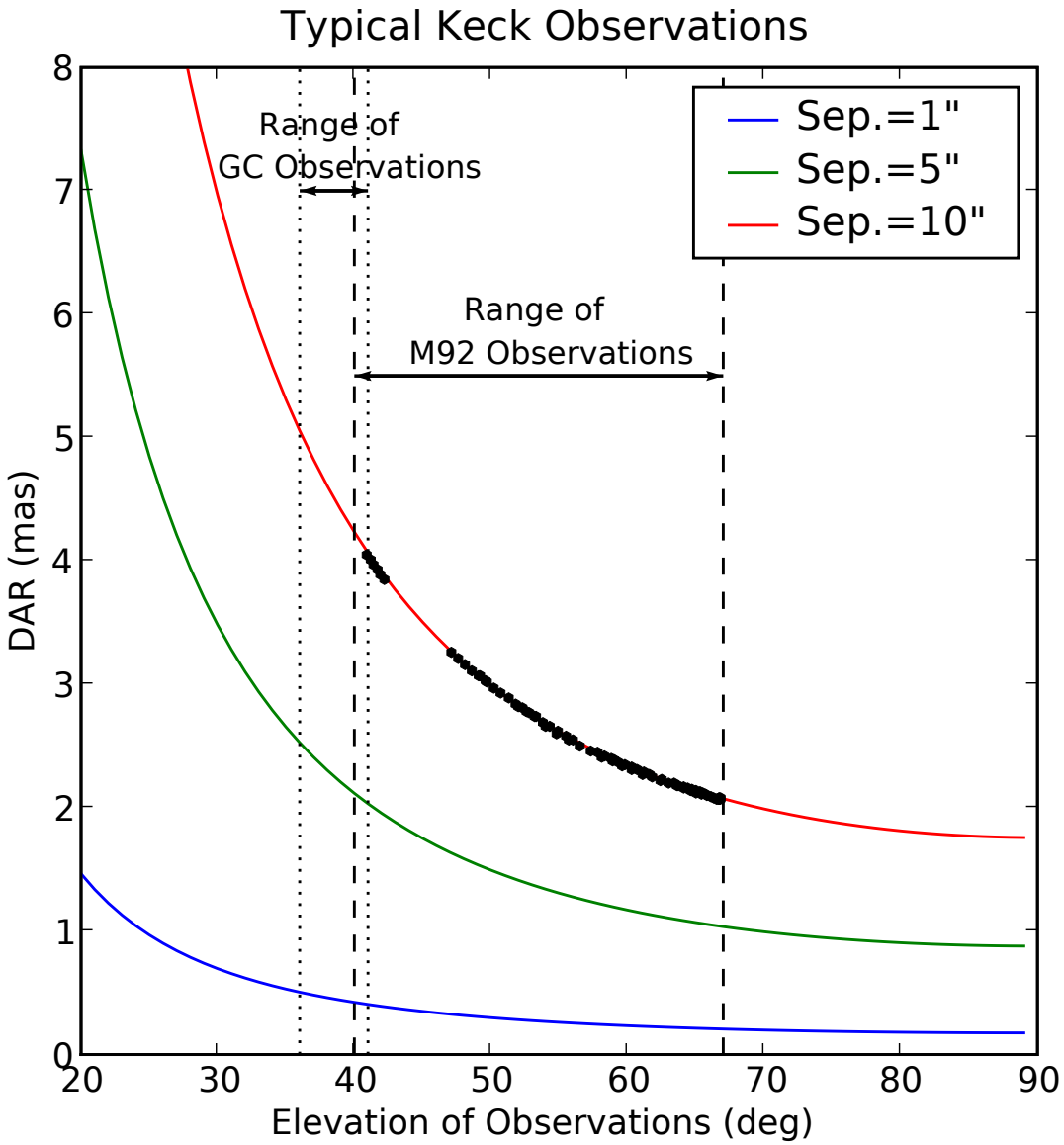

Fig. 4.— The predicted differential atmospheric refraction at a range of elevation angles for *typical* observing conditions at Keck. DAR causes the separation of two stars to appear smaller along the zenith direction and the change in the separation is shown for three pairs of stars separated by 1”, 5”, and 10”. The black dots show the amount of DAR over the 10” field for each of the M92 observations used in the distortion solution. These are offset from the predicted curve (*red*) because the atmospheric conditions differed slightly from the typical conditions at Keck. The range of our GC and M92 observations are also shown.

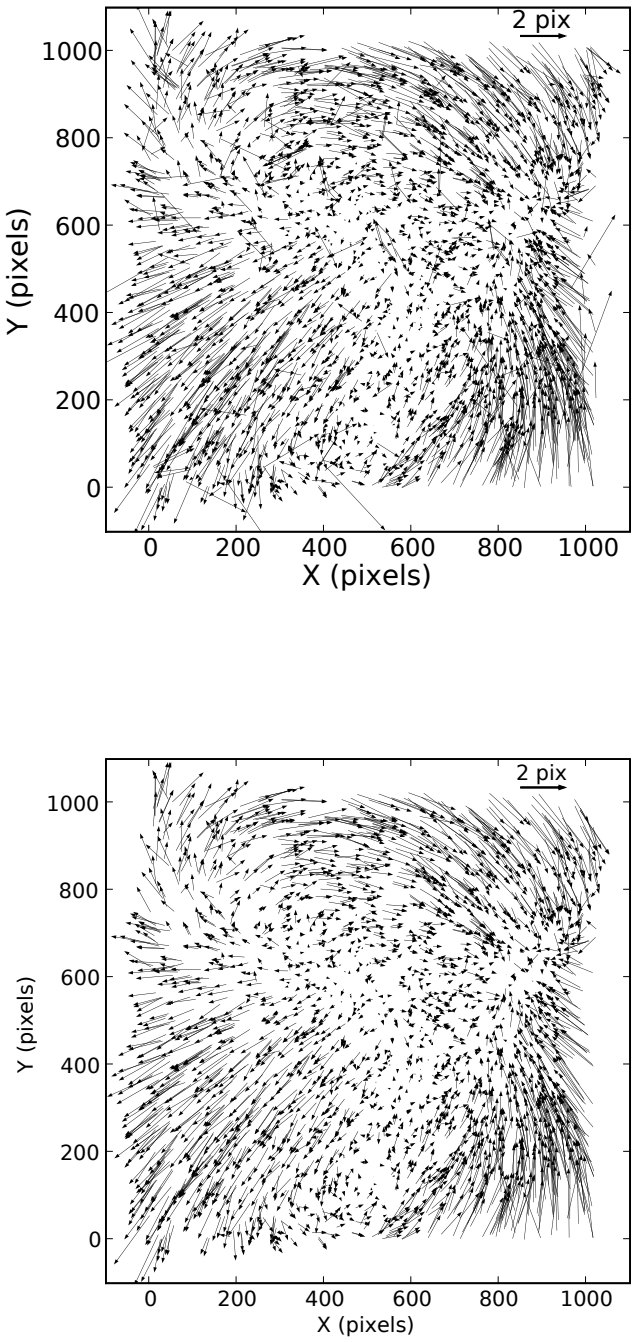

Fig. 5.— Optical distortion in the NIRC2 camera obtained from positional measurements of stars in the globular cluster M92. Arrows indicate the difference between measurements made with NIRC2 (*arrow tail*) and ACS/WFC (*arrow head*), which has a well characterized distortion solution to the ∼0.5 mas level (Anderson & King 2006; Anderson 2007). The two figures show pre- (*top*) and post- (*bottom*) trimming.

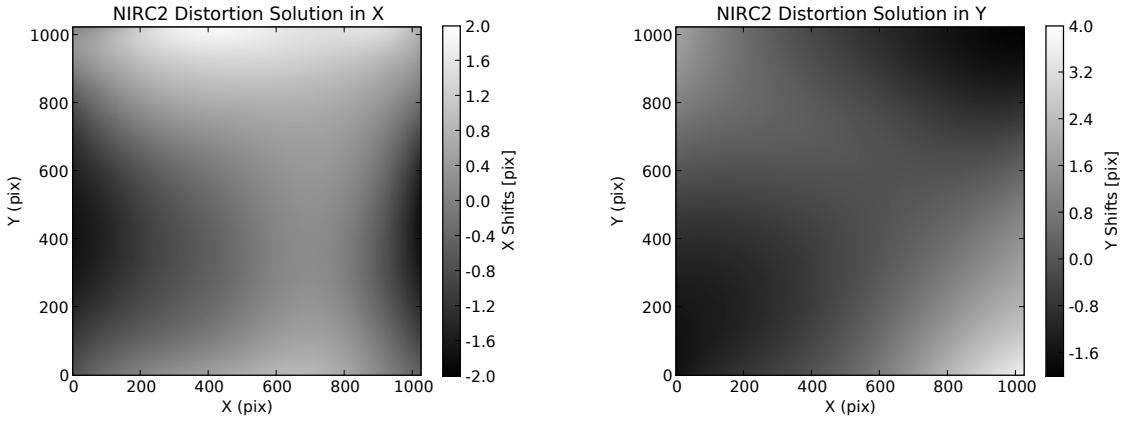

Fig. 6.— Distortion solution in the form of a look-up table for X (*left*) and Y (*right*). The tables gives the X and Y values for each pixel required to remove the optical distortion from NIRC2 images. This was generated by fitting a surface to the distortion map in the bottom of Figure 5. The images are shown in linear stretch.

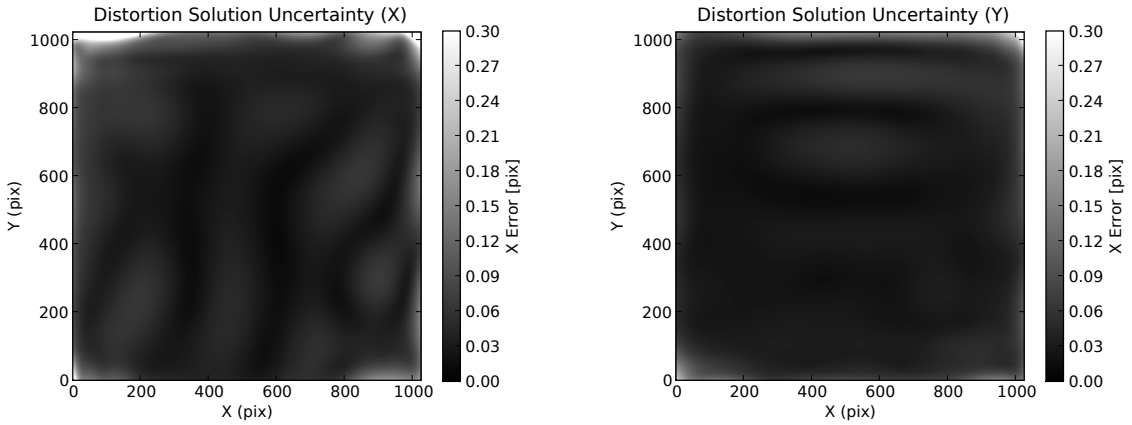

Fig. 7.— RMS error of the 1000 simulations of the distortion solution in FITS file format for X (*left*) and Y (*right*). The images are shown in linear stretch.

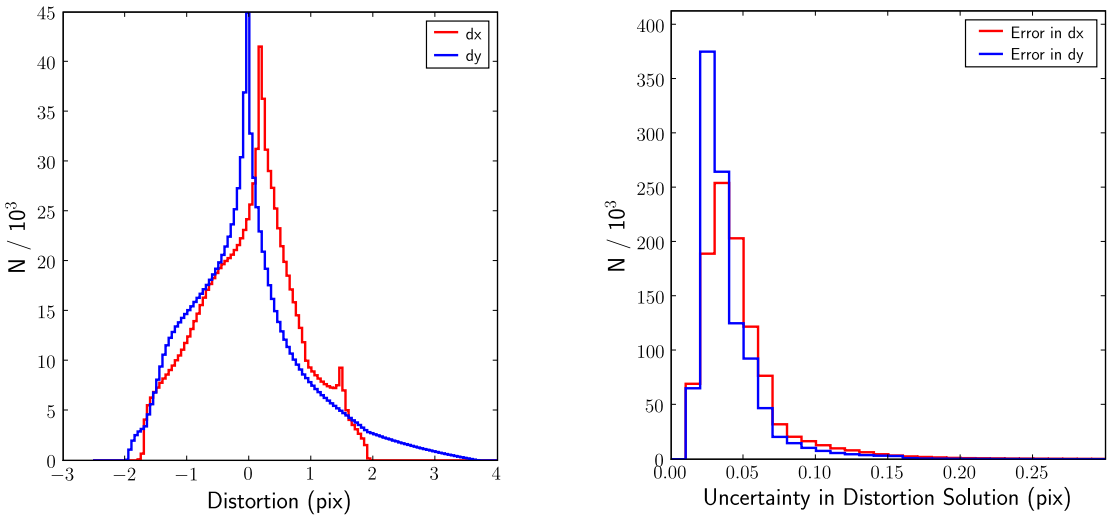

Fig. 8.— (*Left*) Distribution of the shifts in the distortion solution look-up table over all NIRC2 pixels. (*Right*) Distribution of the RMS uncertainties from the 1000 simulations of the distortion solution for X (*red*) and Y (*blue*). The average errors in X and Y are 0.05±0.04 and 0.04±0.02 pix, respectively.

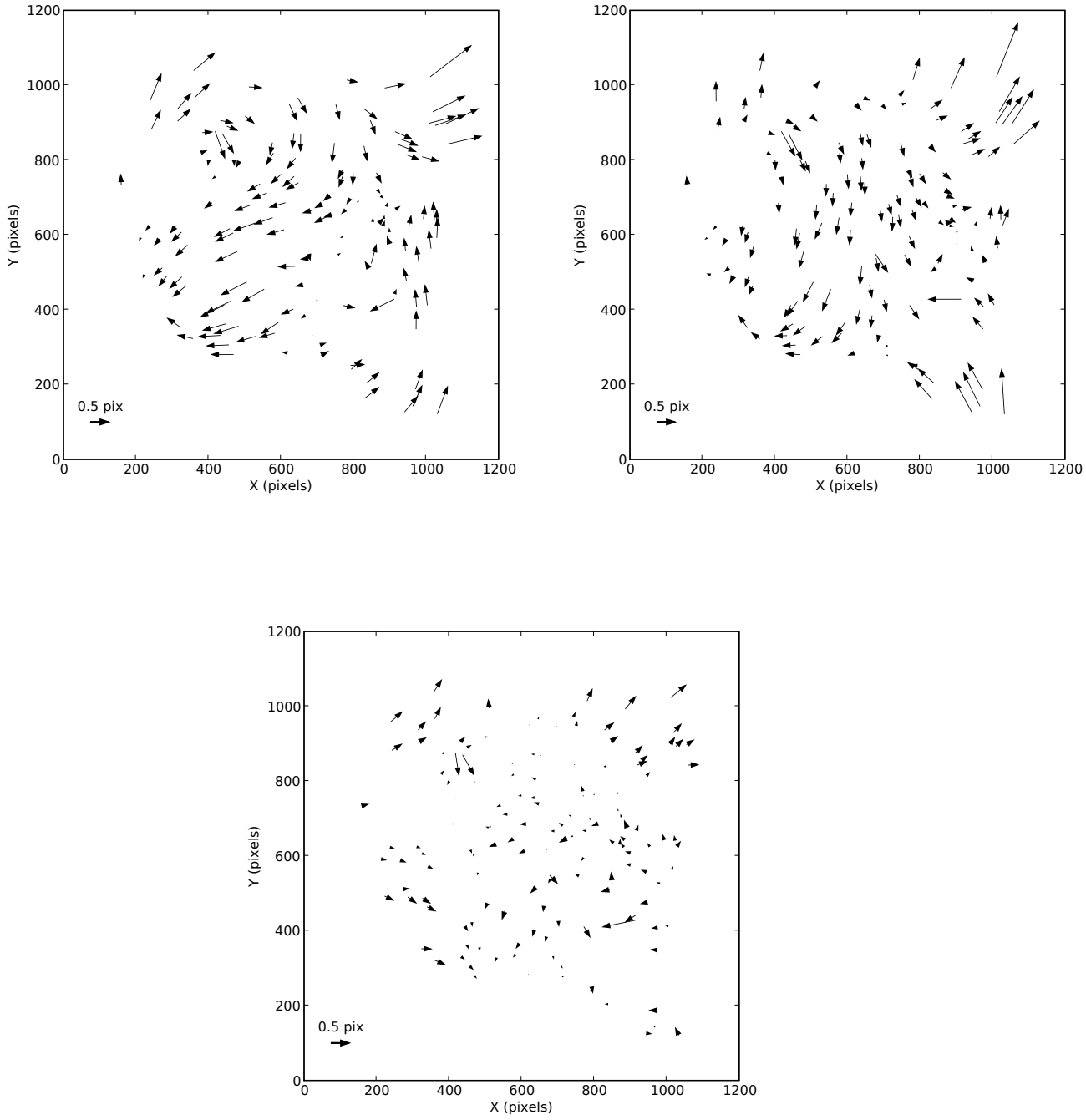

Fig. 9.— Differences between stellar positions in Galactic center images taken at PA=200 (*arrow tail*) and PA=0 (*arrow head*) after applying the pre-ship (*top left*), PBC (*top right*), and the new (*bottom*) distortion solution. While some residual distortion remains, much of the structure seen after using the pre-ship solution is removed with the new solution.

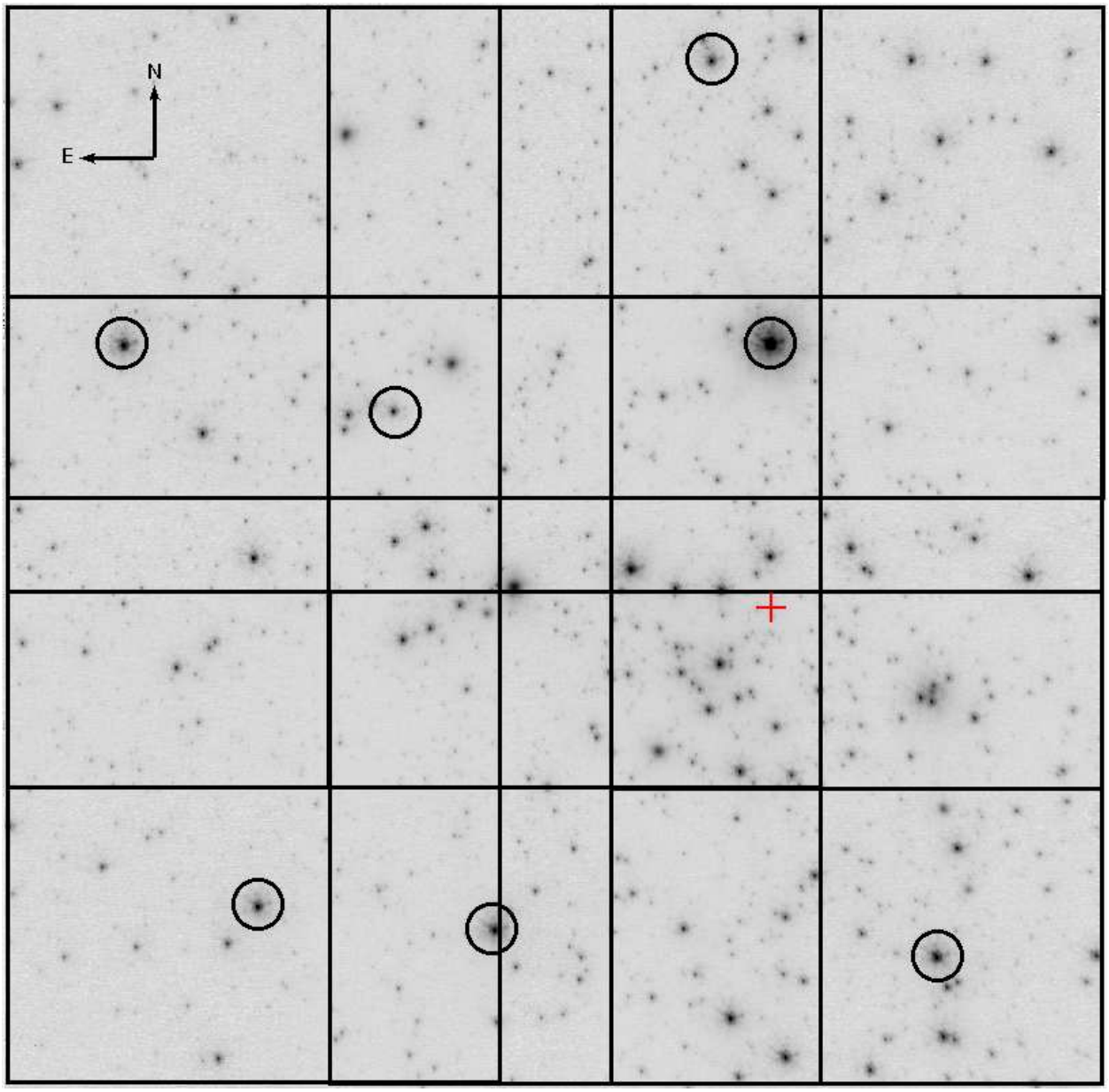

Fig. 10.— NIRC2 K' mosaic image of the Galactic center. The full field is 22"×22", approximately centered on Sgr A* (*red cross*). The black boxes show the nine dither positions making up the mosaic, with each box corresponding to the 10"×10" NIRC2 field of view. The 7 SiO masers used in our absolute astrometry are circled.

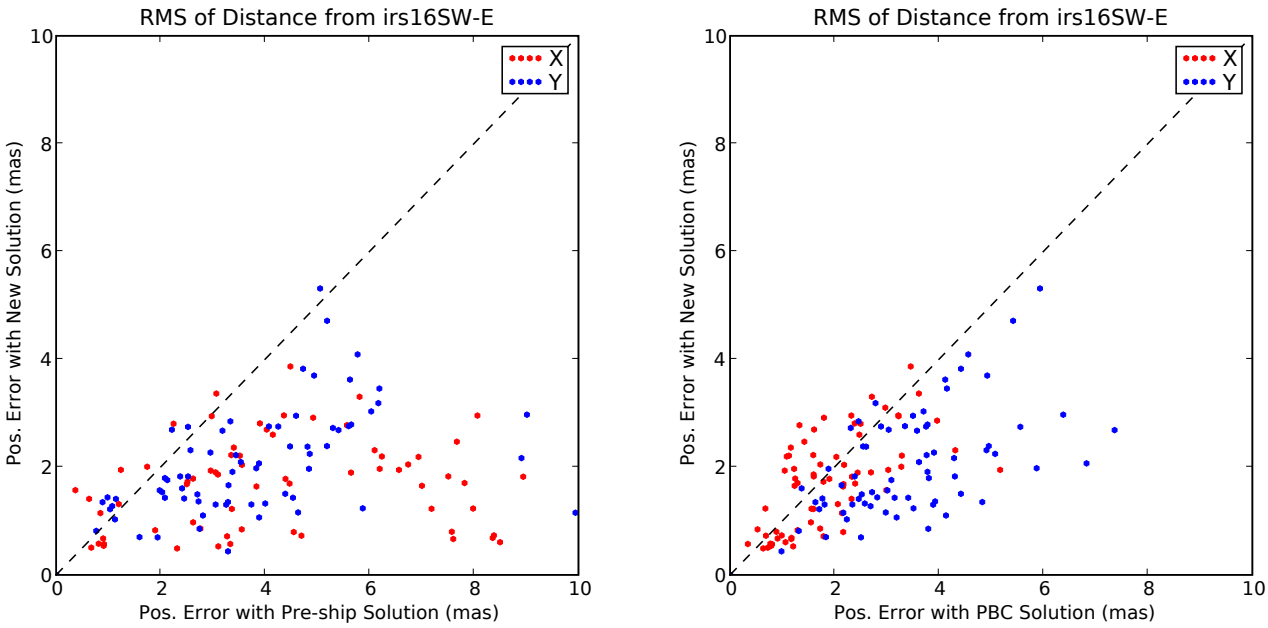

Fig. 11.— Pair-wise analysis on widely-dithered Galactic center data taken in 2006 May. The RMS of the positional offsets from IRS16SW-E are plotted. The plots compare the RMS values from images corrected with the new versus the pre-ship distortion solution (*left*) and the new versus the PBC distortion solution (*right*).

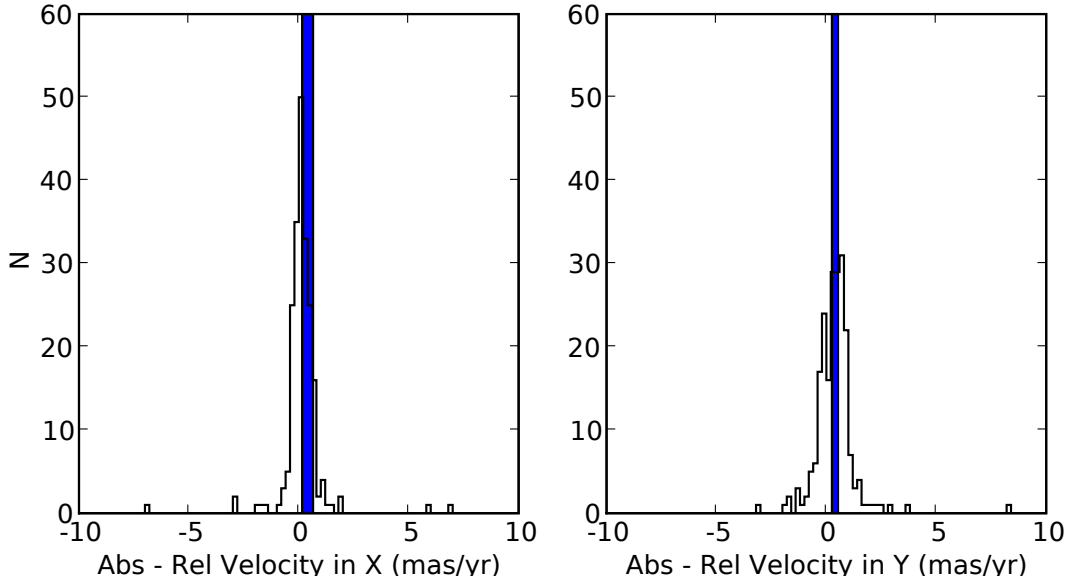

Fig. 12.— Histogram of the difference between absolute and relative velocities of the infrared stars in the Galactic center. The average velocity difference is 0.14 $\pm$ 0.07 and 0.38 $\pm$ 0.06 mas/yr in the East-West and North-South directions, respectively. The vertical bar shows the velocity of the black hole relative to the stellar cluster as derived from the orbit of S0-2 (Ghez et al. 2008).